

Measuring the Reflectivity of the CLAS12 High Threshold Cherenkov Counter Mirrors

Andrew Puckett¹, Youri Sharabian¹, Kyungseon Joo², Nick Markov², Michael McClellan², Harneet Grewal³, Dylan Nicholas³, and John Price³

¹Thomas Jefferson National Accelerator Facility

²University of Connecticut

³California State University-Dominguez Hills

November 2, 2013

Abstract

The CLAS12 High Threshold Cherenkov Counter (HTCC) uses lightweight ellipsoidal mirrors to collect Cherenkov light emitted by fast-moving charged particles in a CO₂ gas volume onto PMTs which measure the light. The mirrors for the HTCC are vacuum-deposited with a reflective coating of aluminum and a protective overcoat of magnesium fluoride or similar material by Evaporated Coatings Incorporated (ECI). The performance specifications of the HTCC require as high as possible reflectivity of the combined coating at ultraviolet wavelengths as low as 200 nm. In order to guarantee the quality of the mirrors used in the final assembled HTCC, a test stand was constructed to measure the reflectivity of HTCC mirrors for wavelengths from 200-650 nm covering the entire range of sensitivity of the HTCC PMTs. This CLAS-note presents details of the apparatus, the measurement procedures and reflectivity results as of mid-August, 2013.

1 Introduction: the CLAS12 High Threshold Cherenkov Counter

The CLAS12 High Threshold Cherenkov Counter (HTCC) is designed to provide highly efficient electron detection as well as high pion rejection power for momenta up to 5 GeV/C by using CO₂ (index of refraction = 1.00045) as radiator. The detector is designed to

subtend a solid angle of 2π in azimuth for polar scattering angles from $5\text{-}35^\circ$. Because the HTCC is located in front of the CLAS12 drift chambers, its material budget is very small; the total thickness of the detector is limited to 200 mg/cm^2 , in order to minimize the disruption of particle trajectories before they are measured. The Cherenkov light emitted by fast-moving charged particles in the HTCC is collected onto 5-inch-diameter photomultiplier tubes (PMTs) located outside the CLAS12 acceptance, surrounding the outer coils of the CLAS12 solenoid magnet.

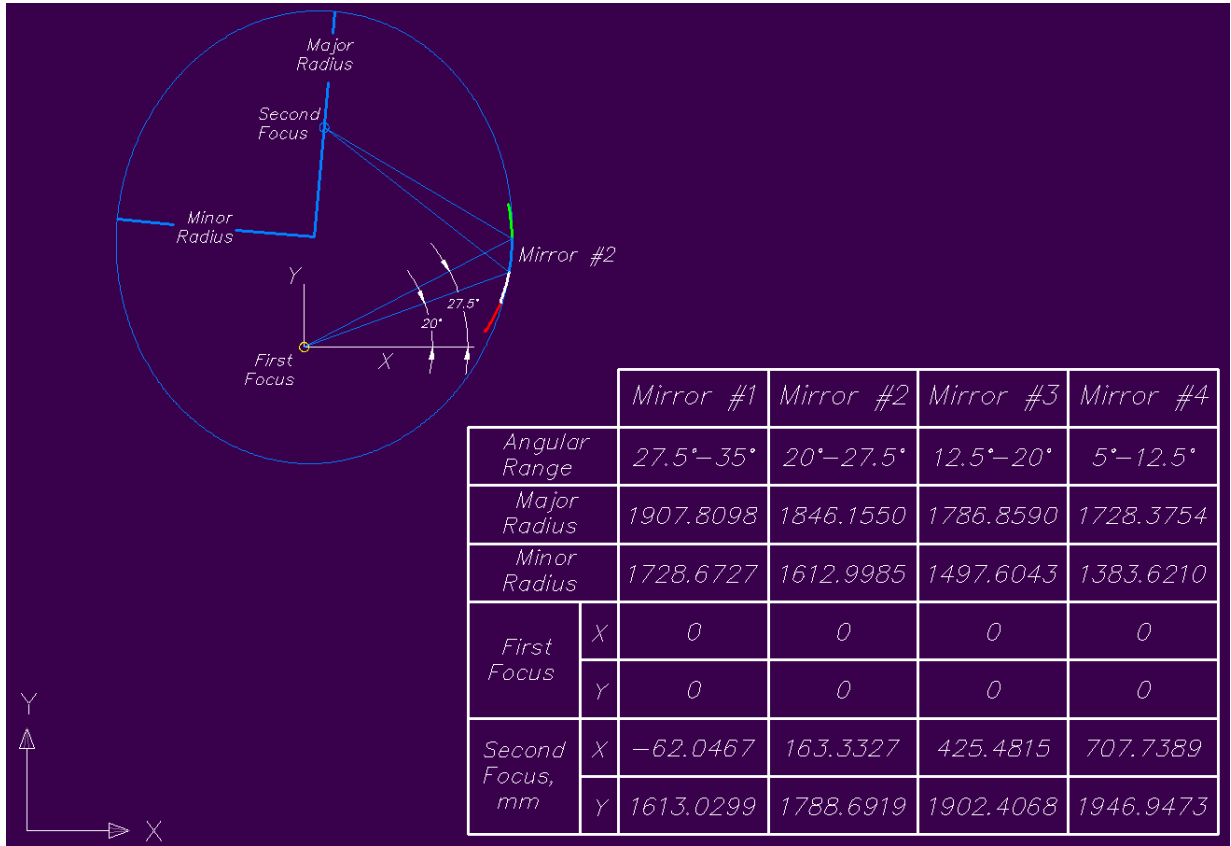


Figure 1: Parameters of the four ellipses. All dimensions are given in mm. In this plot, the x axis is along the beam direction.

Light collection in the HTCC is accomplished by a system of mirrors segmented into twelve “half-sectors” in the azimuthal angle ϕ , where each half-sector is divided into four segments in polar angle θ . The exact geometry of each mirror segment is an ellipsoid of revolution obtained by revolving an ellipse about its major axis. Within each half-sector, each of the four θ segments corresponds to one of four ellipses. All four ellipses share a

common focal point at the origin of CLAS12 and a secondary focus at one of four different PMT locations. The parameters of the four ellipses are shown in Figure 1. The four ellipsoids

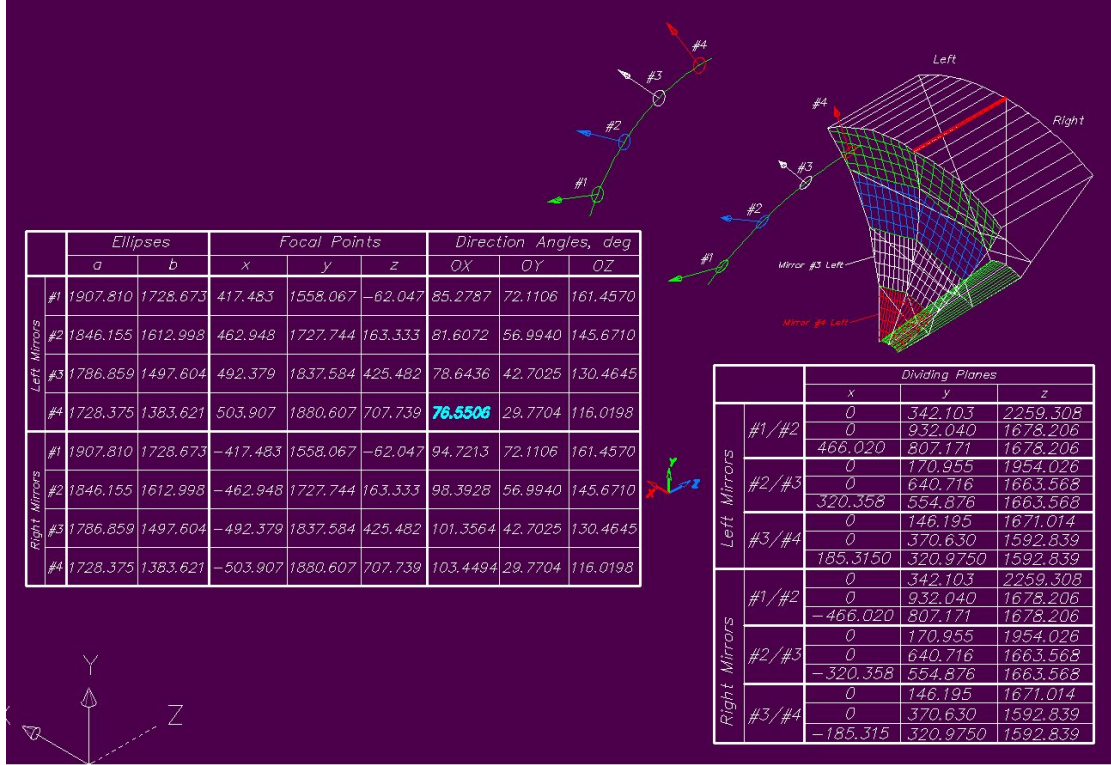


Figure 2: Geometry of two mirror half-sectors combined to form a mirror sector.

of revolution intersect in planes, and therefore the design geometry of the combined mirror covers the entire acceptance with no gaps or shadowing between adjacent mirror facets [1]. Figure 2 shows the combined geometry of two adjacent half-sectors. The individual mirror facets in a half sector are numbered from 1-4 in decreasing order of θ . All twelve half-sectors are identical and each subtends an azimuthal angle range of $\pm 15^\circ$.

The Cherenkov emission angle for $\beta \rightarrow 1$ particles is about 1.7° . The entry window of the HTCC gas volume starts at about 38 cm downstream from the origin, and the path length of particles in the gas averages about 1.4 meters. Light rays originating from one focal point of an ellipse will be reflected by the ellipse surface to the other focal point. Due to the finite emission angle and the continuous emission of photons by each electron along its trajectory, the curvature of the electron trajectory in the magnetic field of the solenoid, and the finite extent of the target, the Cherenkov rays are not emitted exactly as if they came from the origin, and therefore are not reflected exactly to the second focal point of the ellipse. The

distribution of reflected rays near the focal point determines the size of detector needed. 5"-diameter PMTs with quartz windows for high transmission of UV light will be used along with parabolic Winston Cones to increase the light collection efficiency from about 80% to almost 100% (before taking mirror reflectivity into account).

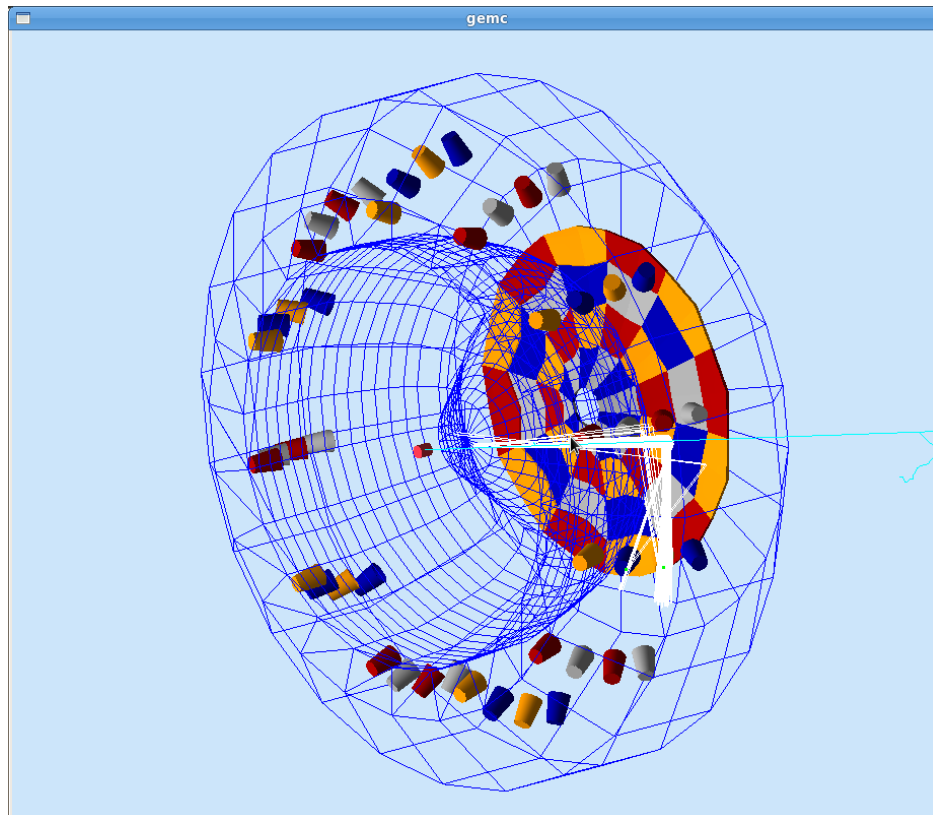


Figure 3: Single-event display from the GEANT4 simulation of the HTCC. The 48 individual mirror facets are shown color-coded to their associated PMTs, shown as thin circular discs representing the PMT photocathodes and parabolic Winston cones. The approximate geometry of the gas containment volume is shown in blue wireframe. The cyan line illustrates the trajectory of an electron going through the HTCC at an angle of 20° , while the white lines are Cherenkov photons emitted by the electron. The rays are reflected by the mirrors to corresponding PMTs. Green dots illustrate PMTs with signals.

Figure 3 shows a single-event display from the GEANT4 simulation of the HTCC. In this example, a single electron goes through the HTCC at $\theta = 20^\circ$ at a random ϕ . The Cherenkov photons, visualized as white lines, are emitted in a cone about the electron trajectory, and are reflected by the mirrors to the associated PMTs, shown as circular discs representing

the photocathodes with parabolic Winston cones that collect rays that otherwise would have fallen outside the active area of the photocathode. In the event shown, the light is shared between two adjacent mirrors, and therefore two adjacent PMTs have signals or “hits”, indicated by green dots.

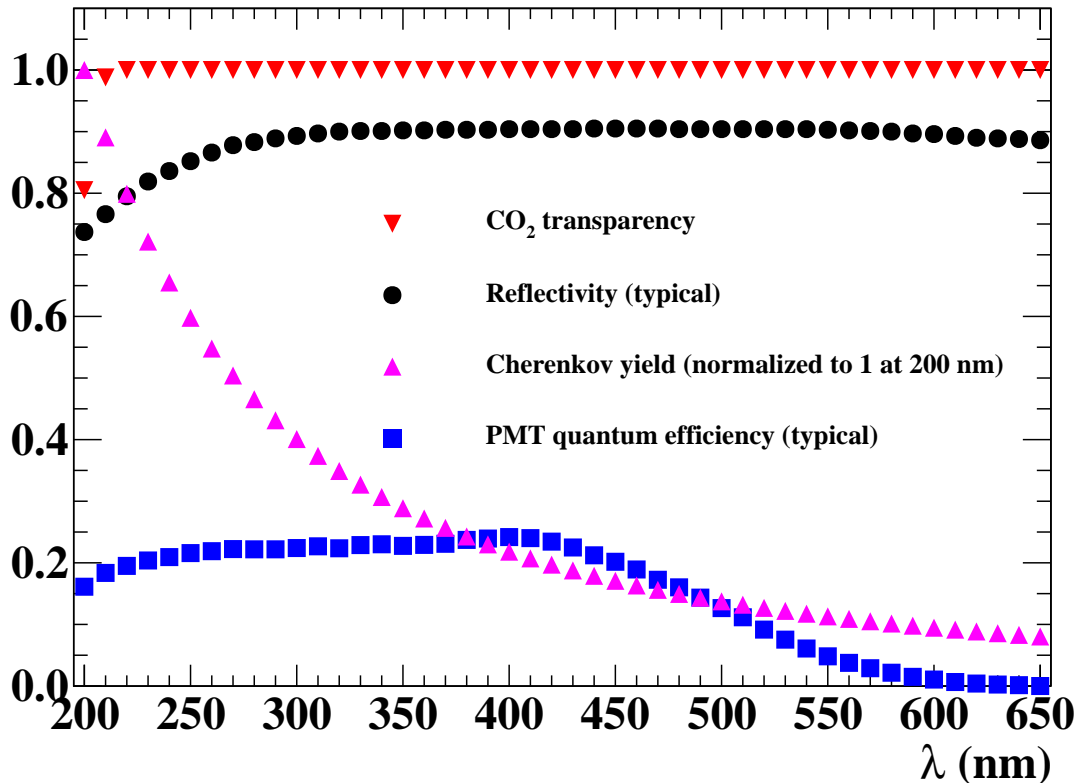


Figure 4: Optical properties of the HTCC that determine the signal strength. The spectral distribution of Cherenkov radiation is normalized to 1 at $\lambda = 200$ nm. A $\beta \approx 1$ particle of charge e emits approximately 18 photons on average over a path length of 150 cm (typical of the HTCC) in the interval $195 \text{ nm} \leq \lambda \leq 205 \text{ nm}$.

The strength of the signal measured by the HTCC is proportional to the number of photoelectrons ejected from the photocathode of the PMT. The number of photoelectrons is determined by the number of Cherenkov photons emitted, the absorption probability in CO_2 , the quantum efficiency of the PMT, and the reflectivity of the mirror used to collect the light. Of course, the number of photons reaching the photocathode also depends on the geometric collection efficiency of the optical system for any given electron trajectory, which is designed to be as close to 100% as possible for interesting electron tracks. Figure 4 shows

typical values of these parameters as a function of wavelength. The spectral distribution of Cherenkov emission is peaked in the ultraviolet, following an approximate $1/\lambda^2$ wavelength dependence in the wavelength regime of interest[2]. The range of sensitivity of the HTCC PMTs with quartz windows is approximately 165-630 nm. Below 200 nm, however, CO₂ is strongly absorptive. Therefore, the region of interest for the HTCC is 200-630 nm. The signal in the HTCC needs to be made as large as possible to provide efficient electron detection at a relatively high threshold and a high pion rejection factor.

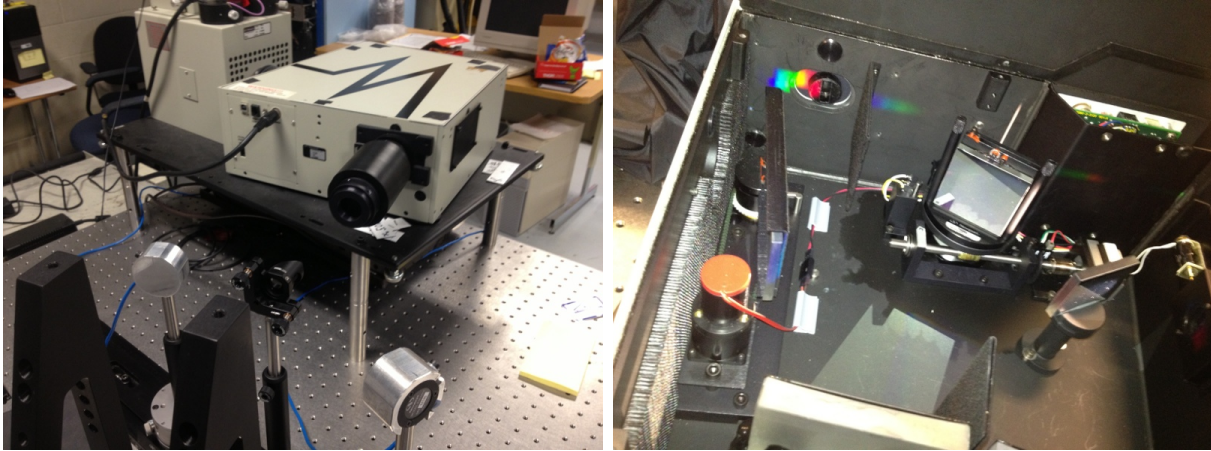
In order not to exceed the small material budget for the HTCC, the mirror facets are constructed from Rohacell31, a special 100% closed-cell foam with a density of approximately 31 mg/cm³. The closed-cell structure of the foam is critical to minimize outgassing under vacuum conditions during the reflector deposition, which can degrade the performance of the reflective coating. The foam is machined to the precise design geometry described above. Due to the large size of mirror 1 and the complicated tooling required for the assembly, each half-sector of the mirror 1 ellipsoid was further subdivided into two mirror-symmetric facets, denoted mirror 1 left and right, obtained by cutting mirror 1 in half along its center line. This means that a total of 60 individual mirror facets will be assembled in the combined mirror. In order to provide structurally rigid mirror substrates with a smooth, optical-quality surface for deposition of a reflective coating, the foam substrates are laminated from both sides with thermally shaped sheets of acryl, epoxied to the foam while being pressed against a precise metal mold with a modest differential pressure of approximately 1.25 psi. To simplify the combined mirror assembly, all four mirror facets have a common back surface shape consisting of a “barrel” obtained by revolving a circle about a chord that is not a diameter, as shown in Figure 5. This shape was chosen to give the most nearly uniform thickness of the foam substrates while simplifying the assembly process.

Evaporated Coatings Incorporated (ECI) was chosen from among four potential vendor companies to perform vacuum deposition of the reflective coating onto the HTCC Mirror Substrates. Two flat sheets of acryl, one untouched and one subjected to the same thermal shaping process used to form the front and back surfaces of the final mirrors, were sent to each of the four companies for deposition. After deposition, the test samples were sent back to JLab and tested for reflectivity using the apparatus described below. The test samples coated by ECI were the most reflective over the entire wavelength range of interest.

2 Mirror Test Apparatus

2.1 Monochromator and light sources

The mirror test apparatus was constructed on a 4×6 ft², 2.4”-thick optical breadboard, supported at waist height by a rigid frame. The breadboard has 48×72 1/4”-20 tapped holes on a 1” rectangular grid. The monochromatic test beam for the reflectivity measure-



(a) Light source apparatus mounted on the breadboard at an optical height of 11.4 inches. (b) Monochromator interior illustrating the dispersion of visible wavelengths from a broadband halogen lamp.

Figure 6: Light source used for the reflectance measurements. Left: The illuminator housing and the monochromator mounted on a common baseplate. The beam exits the monochromator through the collimator, which consists of a pair of 1 mm-diameter pinhole apertures spaced 100 mm apart. Right: The interior of the monochromator viewed from above. White light enters the monochromator from the right through the entrance slit and is collected onto the diffraction grating, which disperses the white light into its component wavelengths. The second spherical mirror focuses the diffracted light onto the exit slit. See text for details.

corresponds to an acceptance cone with an opening angle of approximately 7.4° .

The other important parameter characterizing the monochromator performance is the so-called “reciprocal linear dispersion”, which measures the wavelength-resolving power of the diffraction grating. It is given in units of nm/mm and relates the slit width to the monochromator bandpass. These measurements used a ruled diffraction grating with a line density of 600 mm^{-1} , a reciprocal linear dispersion of $6.4 \text{ nm}/\text{mm}$, and a “blaze wavelength” of 200 nm. The “blaze wavelength” is the wavelength at which the grating is most efficient. The dispersion of $6.4 \text{ nm}/\text{mm}$ means that a 1 mm-wide slit passes a wavelength interval of 6.4 nm, or $\pm 3.2 \text{ nm}$ about the central wavelength. The internal optical design of the illuminator is shown schematically in Fig. 7. The lamp illuminates a spherical mirror which collects as much light as the monochromator can accept. The mirror has a focal length matched to that of the monochromator. Manual external adjustment knobs control the height and orientation of the lamps and the orientation of the spherical mirror, in order to maximize monochromator throughput.

The light diverges from the monochromator in a 7.4-degree cone, with an initial width

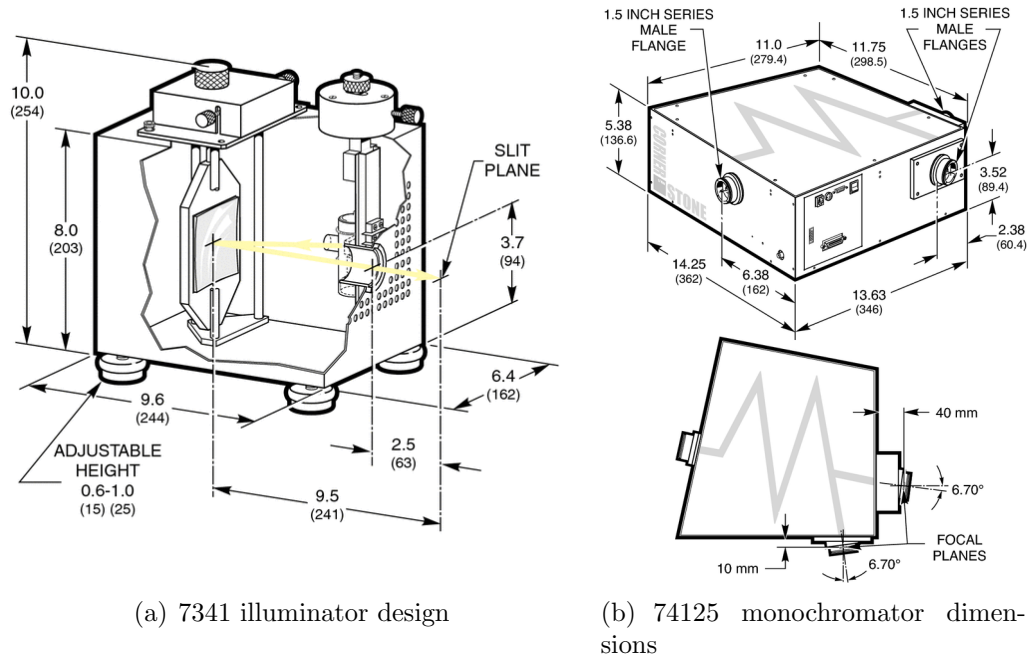


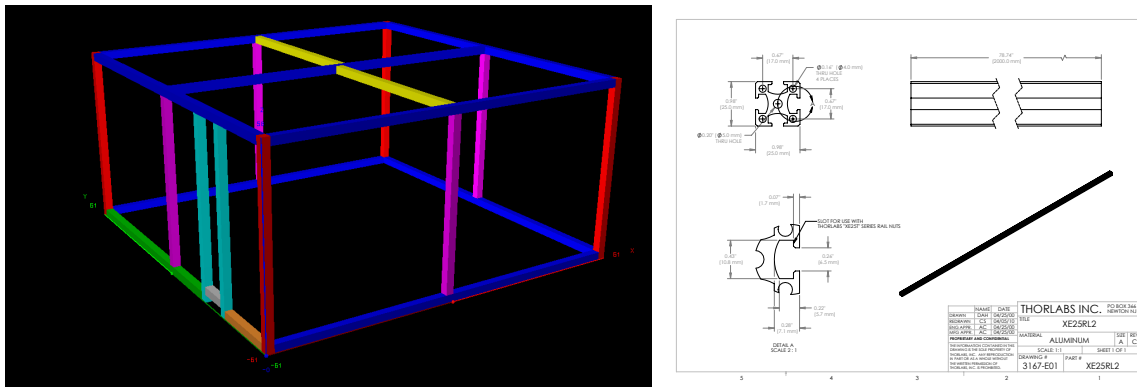
Figure 7: Schematic of 7341 monochromator illuminator (left) and dimensions of monochromator (right).

and height equal to the dimensions of the exit slit (assuming the entire slit area is populated by the source). For mirror reflectivity testing, it is desirable to have a collimated test beam with a small spot size, for several reasons. First, a collimated “point” beam has a well-defined angle of incidence with respect to any given mirror test specimen. Second, the reflectance test method employed involves the use of photodiode sensors to detect the incident and reflected light, and these sensors have a circular area of only 1 cm^2 . Therefore, having a small, collimated beam makes it much easier to collect all the light onto the detector. For these reasons, a collimator was installed at the monochromator exit (the black “tube” protruding from the monochromator box in Figure 6(a)). The collimation is realized using two beam aperture discs, each with a central hole 1 mm in diameter, separated by a spacer tube with a length of 100 mm. The collimator thus limits the beam diameter at the collimator exit to 1 mm and the angular divergence of the beam to about 10 mrad or 0.6 degrees.

2.2 Light-tight enclosure

Given the power output of the D_2 lamp and the acceptance of the collimator relative to the monochromator, the output optical power in the collimated test beam is quite low,

on the order of one to several nW. For this reason, a large light-tight enclosure (hereafter referred to as the “black box”) was built on top of the optical breadboard to provide a low-background environment for the reflectance testing. The structural frame for the enclosure was constructed from 25 mm-square slotted aluminum construction rails, joined together by channel screws. The outer dimensions of the frame are approximately $48 \times 48 \times 23$ in³. The internal clear space is approximately $46 \times 46 \times 22$ in³. The height of the enclosure was chosen to accommodate the largest individual mirror facet (mirror 2) to be mounted inside the enclosure with its central symmetry line oriented horizontally.



(a) Structural frame of the black box. Rails color-coded by length. (b) Design of XE25RL2 aluminum construction rails

Figure 8: Structural frame design of the light-tight enclosure (a) and (b) cross section of the 25 mm square aluminum construction rails used to build the frame. The bottom of the frame rests on the surface of the optical breadboard. The small opening near the bottom of the frame serves as a feedthrough for BNC cables and vacuum tubing. See text for details.

Figure 8 shows the design of the structural frame of the black box. The wall openings were filled using panels of light-weight black hardboard material consisting of a dense foam core sandwiched between plastic-coated cardboard outer layers. The material was available in 5-mm-thick sheets of area 24×24 in². The frame was designed so that each opening could be filled with a single rectangular panel cut from one of these sheets. These hardboard panels fit easily into the 6-mm-wide slots of the construction rails. Each hardboard wall panel was cut to dimensions slightly smaller than the dimensions of each opening plus twice the depth of the channels in the aluminum rails on either side. The corner joints in the rails are such that all side (vertical) wall panels have their entire edges inside the channels of the rails. The three-way joint in the rails at each of the top four corners of the box requires a small cutout to be made at the corner of each ceiling (horizontal) panel. This introduces gaps where light can leak into the black box. These gaps were sealed with black masking

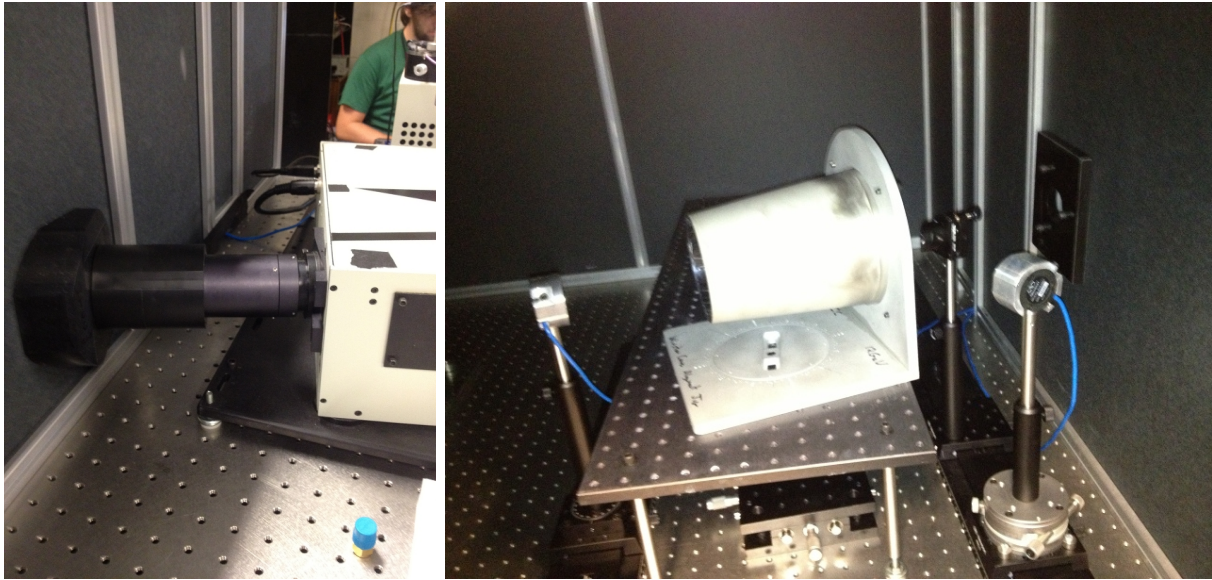
tape, and the entire enclosure was also covered by rubberized blackout fabric. The small opening of dimension $25 \times 100 \text{ mm}^2$ at the front of the box is used as a feedthrough for BNC cables and vacuum tubing for the mirror mounting fixture (see below).

The orientation of the central axis of the collimator relative to the long side of the table is nominally 18.3° when mounted as shown in Fig. 6(a). In order to get the test beam into the black box, an “entry port” was constructed to mate the collimator to the black box. The entry port consists of a black plastic wedge with an angle matching the angle of the collimator with respect to the table, a cylindrical flange perpendicular to the angled surface of the wedge, with a diameter equal to that of the collimator tube, and a cylindrical opening into the black box. The wedge is fastened via three screws to a flat plastic plate from the inside of the black box such that its weight is supported by friction against the wallboard panel. The screw holes in the wallboard panel were cut wide enough to allow for a flexible positioning of the entry port so that it can mate to the collimator with minimal residual stress. The cylindrical flange of the entry port is coupled to the collimator via a black plastic sleeve that blocks external light from entering the enclosure.

Fig. 9 shows how the test beam enters the black box via the entry port. In the photo shown in Fig. 9(a), the entry port was positioned for a beam height of roughly 4.7 inches above the breadboard, a configuration that was used during initial testing of flat sample mirrors. In Fig. 9(b), the interior of the black box is shown during the alignment of a Winston Cone reflectivity test, and the beam entry port is clearly visible on the right interior wall of the black box. To block light leaks through the front cable opening, the bottom of the black box, and other gaps, the entire black box was draped with three large sheets of rubberized blackout fabric, as shown in Fig. 10. A cut was made in one of the sheets so it could be draped around the collimator. Each sheet is $5 \times 9 \text{ ft}^2$ in area. A slot was machined in the vertical rail at the left front corner of the black box so that the side wall panel along the left side of the table could be easily removed to gain access to the inside of the black box without removing the box from the table. This feature was crucially important given the frequent configuration changes required during testing.

2.3 Mirror Vacuum Fixture

To test the HTCC mirrors, they must be positioned in the path of the test beam inside the black box. Given the delicate nature of the reflective coating and the complicated geometry of the mirror facets, it was necessary to design a custom fixture to mount the mirrors on the optical table for reflectivity testing, without contacting the reflective surface. Exploiting the common back surface shape of all five mirror facet geometries, a single vacuum fixture was designed to mount all five mirror facets interchangeably by machining a smooth indentation into an aluminum plate corresponding to a small section of the barrel shape. Strictly speaking, because the barrel shape is obtained by revolving a circle about a chord that isn't a diameter (see figure 5), rotational symmetry is broken, and the surface shape is



(a) Beam entry port from outside the black box

(b) Beam entry port as seen from inside the black box.

Figure 9: 9(a): Black box entry port with removable sleeve coupling the collimator to the black box. This picture shows the configuration that was used in early tests of flat sample mirrors, with a beam height of approximately 4.7 inches. In the final configuration with a beam height of 11.4 inches above the breadboard, the same hardware was attached to another wallboard panel with a hole at the appropriate height. 9(b): Black box interior during alignment of a Winston cone test. The beam entry port is visible on the right wall.

not invariant with respect to rotations about the circular arc corresponding to the mirror center line, as it would be if the shape were spherical. However, because the shape is very close to spherical within the angular extent of a half-sector, the deviations from an exact fit for each facet are very small, and were calculated to be less than 0.001" over the entire area of vacuum engagement of the fixture, which is defined by the smallest mirror facet (number 4). Deviations at this level are well below the tolerances for manufacturing of the facets themselves and were therefore neglected.

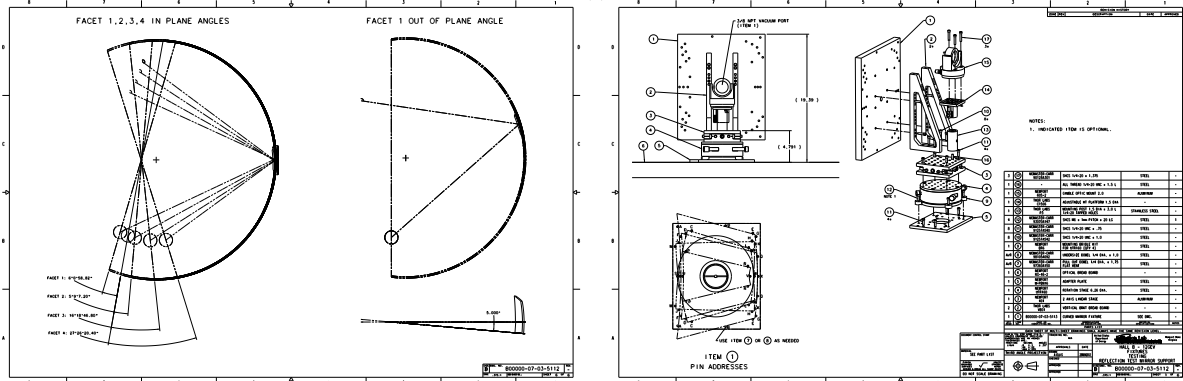
Fig. 11(a) shows the rotation angle of each facet along the circular arc corresponding to the half-sector center line, relative to the location chosen to define the curved surface of the vacuum fixture. The final positions of mirrors 2, 3 and 4 on the vacuum fixture are obtained by a rotation along the half-sector center line, such that both focal points of the corresponding ellipses are in a horizontal plane at beam height. Because mirror 1 is split along the half-sector center line, mirror 1 left and right also had to be rotated by equal and



Figure 10: The black box in a typical measurement configuration. (a) The view from the left side of the table, showing the collimator coupled to the beam entry port. The picoammeters used to measure the photocurrent during the tests fit conveniently below the monochromator mounting platform. (b) The view from the right side of the table, showing the back of the illuminator with cooling fan and the cart housing the lamp power supplies and the diaphragm pump used to hold the HTCC mirrors against the vacuum fixture inside the black box.

opposite out-of-plane angles in order to be accommodated by the fixture. For these facets, because the out-of-plane rotation is with respect to the rotated barrel axis, which passes through the origin, the focal point corresponding to the origin of CLAS12 remains at the same height, but the focal point corresponding to the PMT location is shifted slightly down (up) for mirror 1 left (right).

Fig. 11(b) shows the hardware used to mount the vacuum fixture on the optical table. A Newport model UTR160 steel rotation platform was used to provide 360-degree rotational freedom of the fixture about the vertical axis. This platform is engraved with a Vernier scale with arc-minute angular resolution. A Newport model 401 two-axis linear translation stage was mounted on top of the UTR160 to provide horizontal translation of the fixture with 13 mm of travel, driven by micrometers with one-micron resolution. Right-angle brackets were used to attach the vacuum fixture to the surface of the translation stage. A 1.5"-diameter steel post and an adjustable-height mounting platform were used to support a model 605-2 precision gimbal mount from Newport on the opposite side of the translation stage. The gimbal mount is used to mount standard 1"-diameter optics, and is predominantly used for alignment activities and control measurements using a standard reference mirror with specified flatness and reflectivity. Fig. 12 shows an actual photo of the mirror vacuum fixture

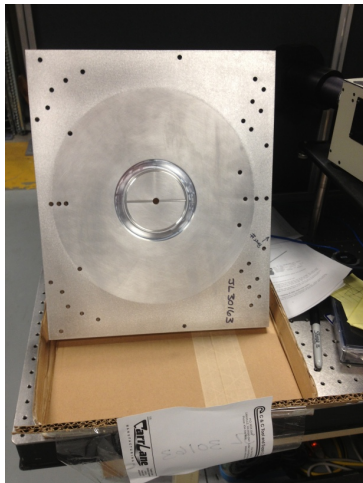


(a) Mirror nominal positions relative to final positions on the vacuum fixture. (b) Assembly of mounting platform used to mount the fixture to the optical table.

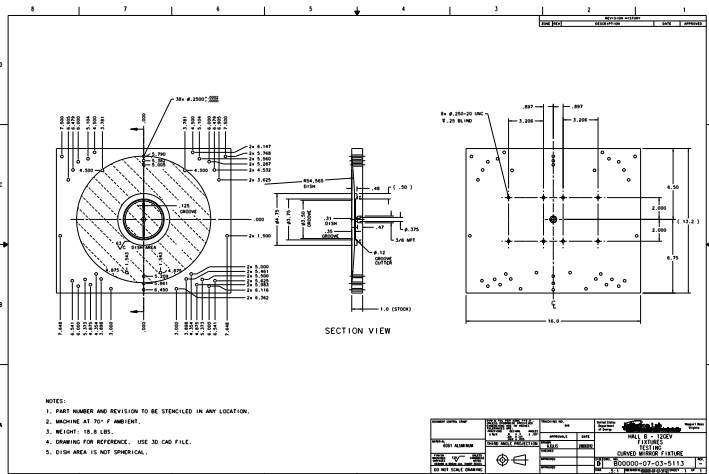
Figure 11: (a) Rotation angle of each mirror facet from its nominal position in a half-sector to its final position on the vacuum fixture. Because mirror 1 is divided into left and right facets along its center line, the mirror 1 facets must also be rotated by 5 degrees out-of-plane. (b) The hardware used to mount the vacuum fixture vertically on the optical table. See text for details.

before mounting on the optical table and the basic design parameters of the fixture. The area of vacuum engagement is defined by the circular 0.125” groove connected by two “spokes” to the central vacuum port. The diameter of this groove is 3.5 inches. The outer groove can be optionally used to hold a gasket, but experience has shown that the mirror back surface fit is good enough for the vacuum to hold with no significant leaks, even without a gasket. A set of location pins is used to repeatably position each mirror facet on the vacuum fixture. 1/4”-diameter undersized removable dowel pins are inserted for each mirror facet according to the hole patterns shown in Figs. 13(a) (mirror 1 left and right), 13(b) (mirror 2), 14(a) (mirror 3), and 14(b) (mirror 4). These drawings also show the locations of the corresponding ellipse focal points relative to the center of the UTR160 rotation platform, for a specific assumed orientation angle of the platform relative to the optical table. From these drawings, the positions of the mirror focal points can be calculated for any position and orientation of the platform, which in turn allows the calculation of the angle of incidence and other properties of the incident and reflected beams in any given mirror test.

The vacuum is applied to the mirror holding fixture by a dual/parallel head diaphragm pump with a capacity of 2.2 cfm equipped with pressure gauges, regulators and a relief valve. The pump is typically regulated to a differential pressure of about 1/3 of atmosphere. Given the area of vacuum engagement, this implies that the mirror is held against the fixture by a force of roughly 50 pounds. The pump is located outside the black box and connected to



(a) The actual vacuum fixture after fabrication at the JLab machine shop.



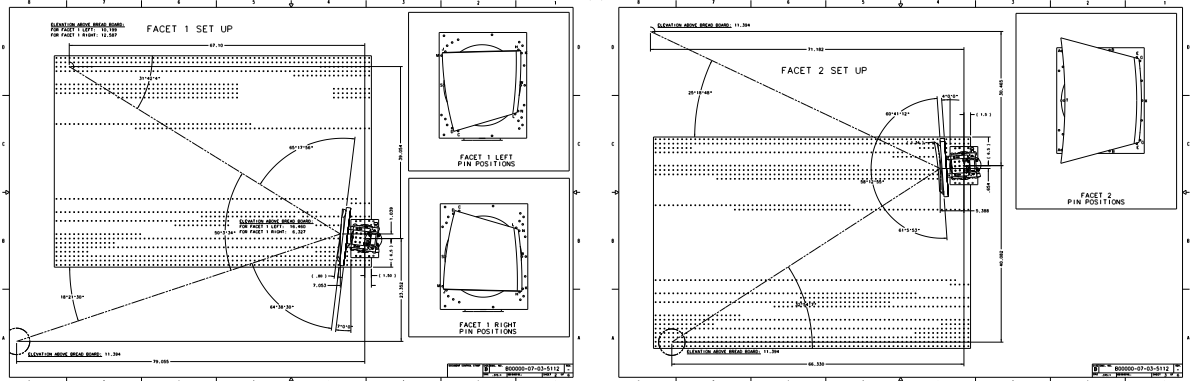
(b) Design specifications of the curved fixture.

Figure 12: (a) The actual vacuum fixture before mounting on the optical table. (b) Design specifications for the curved vacuum fixture (for reference only).

the back of the mirror fixture by approximately 20 feet of flexible thick-wall vacuum vinyl tubing with a 3/8" ID and 7/8" OD. The tubing is attached to the back of the vacuum fixture via a 3/8" male NPT hose connector with a 3/8" ID hose barb. Fig. 15 shows the typical use cases for the vacuum fixture. In Fig. 15(a), a coated mirror 1 left is held against the fixture by vacuum. In Fig. 15(b), a flat mirror is mounted on the opposite side of the platform using the gimbal mount.

2.4 Alignment laser

A Newport model LOA-2 diode laser was used to align all components on the optical breadboard for all measurements. The power of the laser is 2.7 mW, its central wavelength is 635 nm, and its safety class is 3R. In order to make the laser safer to use for alignment, it was enclosed in a lens tube and capped with a neutral density filter with an optical density of 1.0 (implying 10% transmission), which reduces the power to well below 1 mW. During alignments, the laser was placed inside the monochromator enclosure, suspended from a large plexiglass plate that rests on top of the walls of the enclosure with the lid removed. The laser was mounted via two screws used to adjust its elevation and pitch. The laser's yaw angle and position were adjusted by manually moving the plate. The laser aim was adjusted until the beam passed through both apertures of the collimator with maximum brightness.



(a) Location pin positions and focal point locations for mirror 1 left and right (b) Location pin positions and focal point locations for mirror 2

Figure 13: Location pin configuration and focal point positions for mirror facets 1 and 2.

In this way, the beam used for alignment was made to coincide with the test beam emerging from the monochromator.

2.5 Photodiode sensors, focusing lens assemblies and picoammeters

The optical power of the incident and reflected light during mirror tests was measured by a pair of Newport model 818-UV-L UV-enhanced silicon photodiode sensors. Each sensor was delivered with a NIST-traceable calibration report, where the calibration was performed at a temperature of 22 °C. The relevant performance specifications of these photodiodes are linearity, uniformity, calibration uncertainty and the so-called noise-equivalent power (NEP), which provides a measure of the minimum optical power that can be measured. For these sensors, the linearity specification is $\pm 0.5\%$ within the linear region of the sensors, which ranges from the NEP of $0.45 \text{ pW}/\sqrt{\text{Hz}}$ to the maximum measurable power of 0.2 mW (without an attenuator). Above the maximum power, the measured photocurrent begins to saturate, and is no longer proportional to the incident power. Figure 16 shows the linearity and temperature performance characteristics of various photodiodes in the 818 series. The uniformity of the photodiodes is $\pm 2\%$, meaning that the responsivity may vary across the photodiode surface by up to 2%. The active area of the photodiode is circular, with an area of 1 cm^2 .

The two photodiodes used for the measurements have serial numbers 12141 and 12145, respectively. Their responsivities are shown in Fig. 17. In the region of interest for the HTCC PMTs, the responsivities of the two photodiodes are virtually identical, while the responsivity

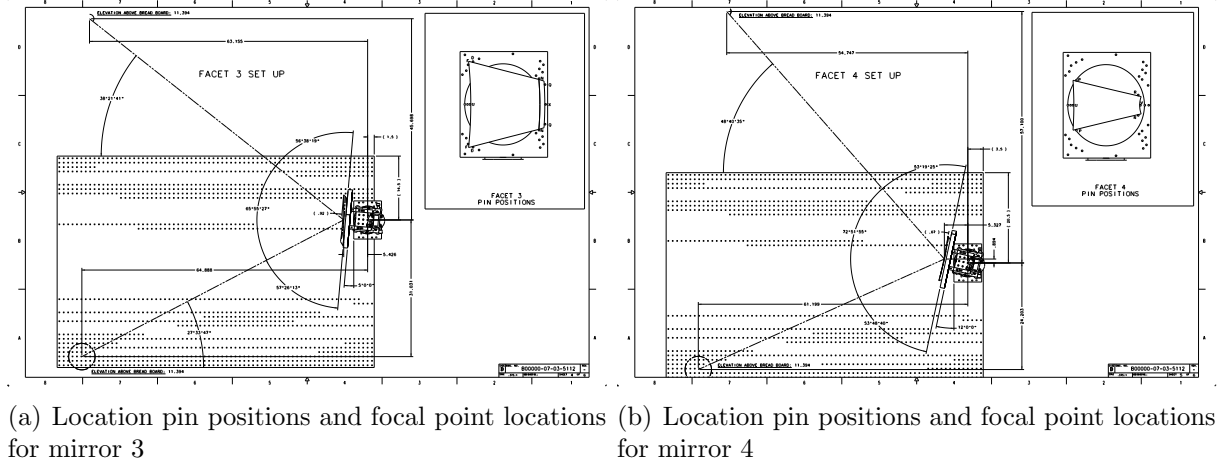
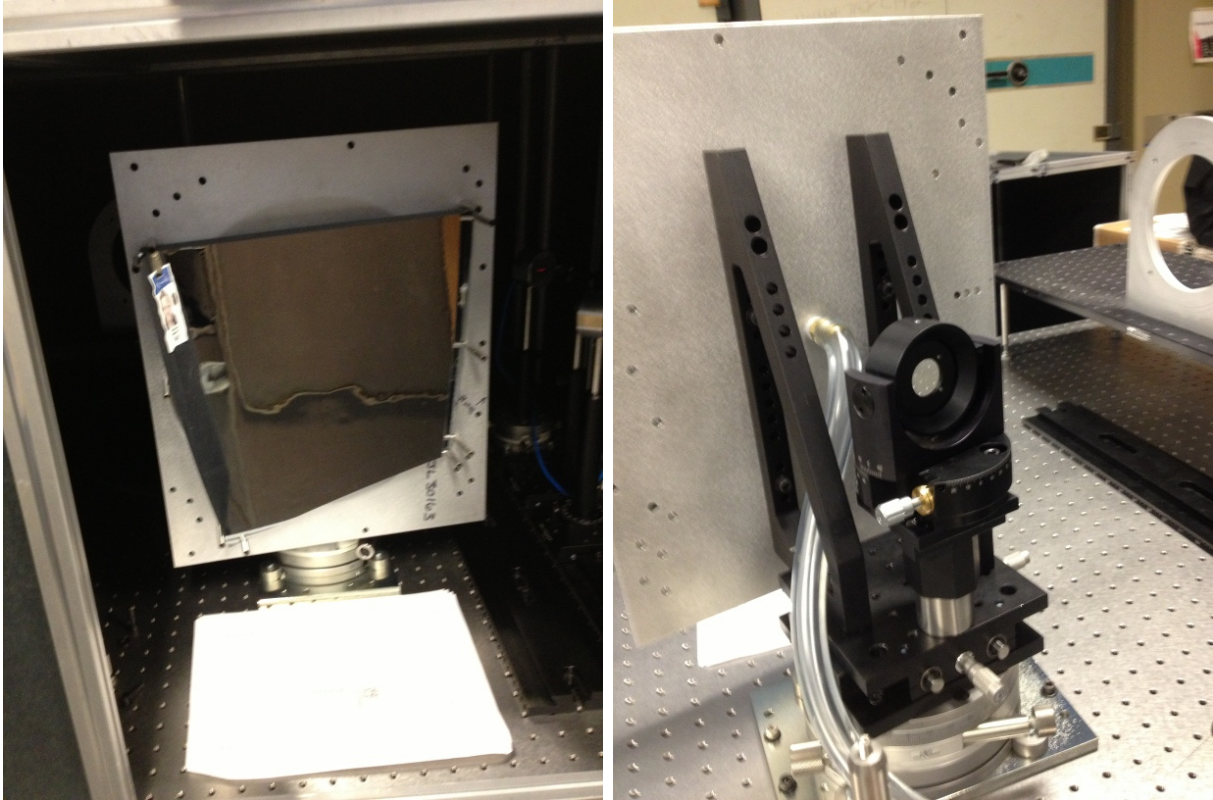


Figure 14: Location pin configuration and focal point positions for mirror facets 3 and 4.

of the photodiode with S/N 12145 exceeds that of S/N 12141 in the infrared. The photodiodes come with preattached coaxial cables and male BNC connectors. The photocurrents were measured using two Keithley model 485 auto-ranging picoammeters capable of measuring currents as low as 0.1 pA.

Fig. 18 shows a typical example of the power level in the test beams produced by the two lamps. In this example, the two detectors measured the light reflected and transmitted by a beam splitter. The curves shown represent the sum of reflected and transmitted light, and do not account for losses in the beam splitter or in the fused silica lenses used to focus the incident light on the photodiodes. The power reaching the photodiodes is determined by many variables, including the spectral distribution of lamp output, the throughput of the monochromator as a function of wavelength, the acceptance of the collimator, the reflectance, transmission and absorption of the beam splitter and the transmission of the focusing lens (if applicable). The monochromator throughput depends strongly on the alignment of the lamp and the mirror inside the illuminator housing, the area of input and output slits, the reflectivity of the mirrors and the efficiency of the diffraction grating. Despite significant output of the D₂ lamp down to 180 nm, the measured power falls off strongly below 230 nm, mainly due to high reflectance and low transmission of the UV beam splitter coating, which is only “rated” for a wavelength range of 250-450 nm. Owing to the small acceptance of the collimator relative to the monochromator itself, the test beams are weak in absolute terms; but more than strong enough for the photodiodes and current meters involved. At 400 nm, the measured power from the D₂ lamp is about 0.4 nW, which is almost 1000 times the NEP. Moreover, power levels of 1-10 nW as shown in Fig. 18 are comfortably within the linear region of the 818-UV.



(a) The first-article mirror 1 left #12 mounted on the vacuum fixture with location pins. (b) The flat control mirror gimbal-mounted behind the vacuum fixture.

Figure 15: The mirror vacuum fixture mounted on the optical table with (a) the first HTCC mirror deposited with a reflective coating (mirror 1 left, #12) and (b) the flat “control” mirror used for alignment and to check systematics of the measurements.

In order to measure the reflectivity of a given mirror, 100% of the light transmitted by the beam splitter needs to be collected during the calibration and 100% of the light reflected by the mirror needs to be collected onto the photodiode during the measurement¹. 100% collection efficiency for light reflected by the beam splitter is not strictly required as long as the collection inefficiency is constant between the calibration of the beam splitter and the reflectivity measurement. Because the beam is allowed to diverge after leaving the collimator, the spot size increases with optical path length. At the collimator exit, the test

¹In principle, reflectivity can be measured with less than 100% collection efficiency if the collection inefficiency is known or is constant. In practice, however, the collection inefficiency cannot be held constant or determined with sufficient accuracy.

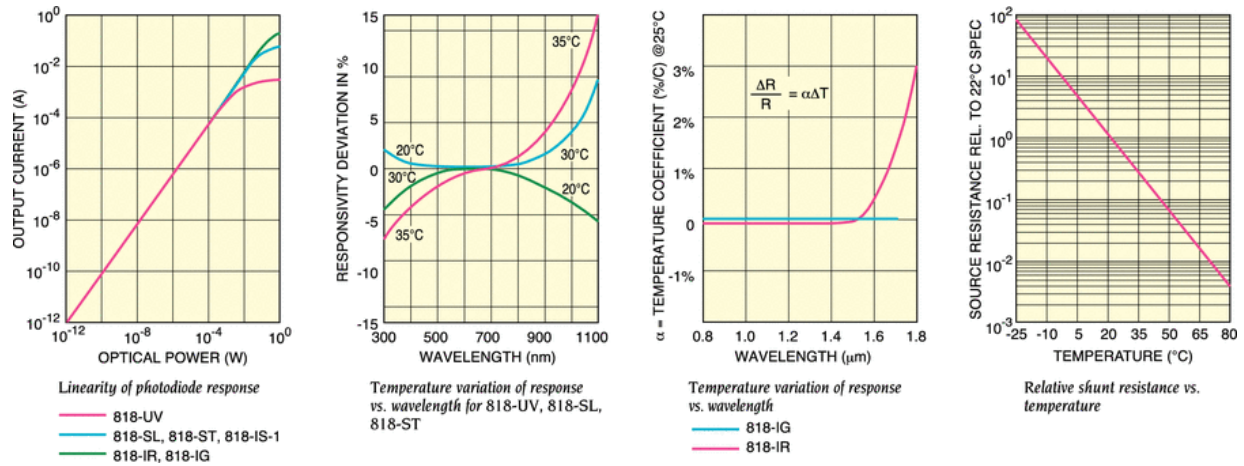


Figure 16: Linearity and temperature-dependent performance characteristics of Newport model 818-UV-L silicon photodiode sensors.

beam diameter is 1 mm. The maximum angle that can pass through the collimator is 0.6° ; therefore, the maximum spot size increases by about 3 mm per foot of optical path length after the collimator exit. Because the diameter of the active area of the photodiode surface is 11.3 mm, reliable measurements can only be done over relatively short path lengths. In order to circumvent this limitation, focusing lenses were used to increase the effective collection area of the photodiode by a factor of approximately four. Two identical lenses with a focal length of 100 mm were used. The lenses are made of uncoated UV fused silica with a plano-convex spherical geometry, are 1 inch in diameter, and have an index of refraction of 1.460 at 590 nm. Fig. 19 shows the photodiodes, the beam splitter and the focusing lens assemblies during a typical beam splitter calibration measurement. Each lens is mounted in front of its respective photodiode in a threaded holder that provides up to 0.8 inches of travel along the optical axis for focus adjustment. Each lens-photodiode assembly shown in Fig. 19 is mounted on a rotatable platform, which in turn is mounted on a rail carrier, allowing for rotation about the vertical axis and translation in one horizontal direction. Moreover, the vertical post that holds the entire assembly is height-adjustable. The optical axis of the lens-photodiode system is always horizontal when mounted using the hardware shown in Fig. 19. This configuration works best for horizontal or near-horizontal beams, but is impractical for beams with significant vertical slope. Though the hardware can easily be modified or rearranged to provide vertical tilt of the optical axis, it is not typically necessary to do so because the incident and reflected test beams are in a horizontal plane. The exception to this is the testing of mirror facets of type 1 (left and right), for which the reflected beam has a vertical slope on the order of one degree, leading to a small vertical offset of the focused beam spot at the photodiode. The detector that views the light reflected by the beam

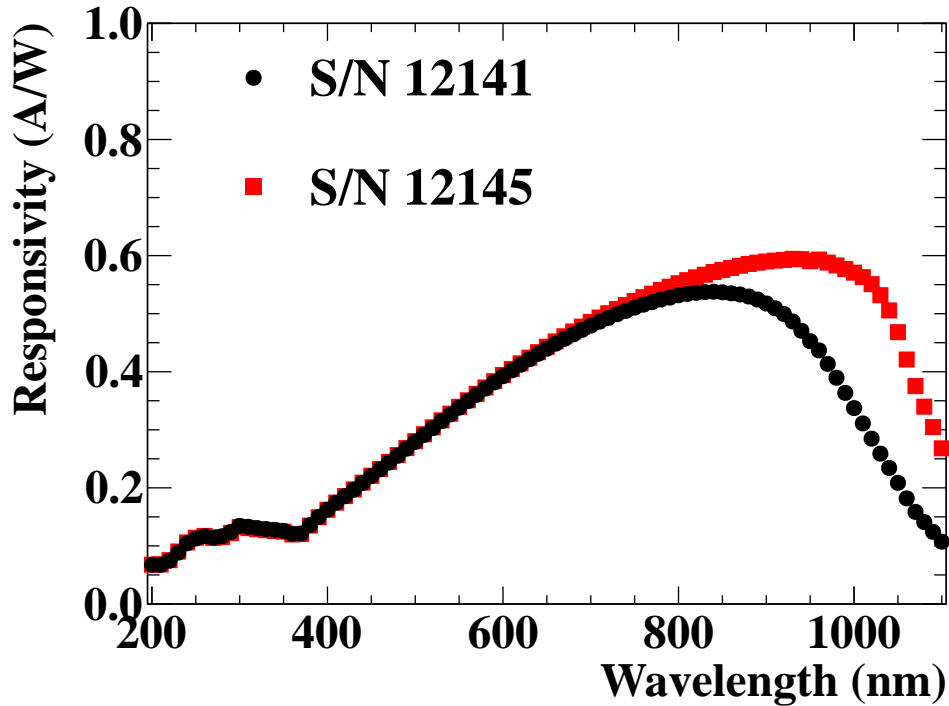


Figure 17: Photodiode responsivities in Amps/Watt, according to the calibration reports provided by Newport.

splitter is mounted on a Newport model UTR80 precision steel rotation platform with an angular resolution of 1 arc-minute. The precision of this platform is instrumental in aligning the beam splitter for 45° AOI. The detector that views the transmitted light during the calibration and the mirror-reflected light during each test is mounted on a Thorlabs model RP01 rotation platform, which has 2-degree angle graduations.

The laser beam used for alignment has a power of 0.27 mW (after passing through the OD1.0 filter), and a peak power density of order 10 mW/cm². Although this power level will most likely not damage the photodiode, it is a good practice not to expose the photodiode, which is used to measure nW-level signals, to such high-intensity light. Moreover, the power density increases significantly near the focus of the lens, which could potentially damage the photodiode surface locally. To avoid exposing the photodiode surfaces to the laser light during alignment, frosted glass alignment discs were used to locate the correct position and orientation of the lens tube and then the photodiodes were secured in place after the laser had been turned off, as shown in Fig. 19. These discs are made of 1500-grit ground glass with a 1 mm-diameter center hole, mounted in a threaded holder that threads into either end of the lens tube. The frosted glass diffuses the visible laser beam, so that the deviation

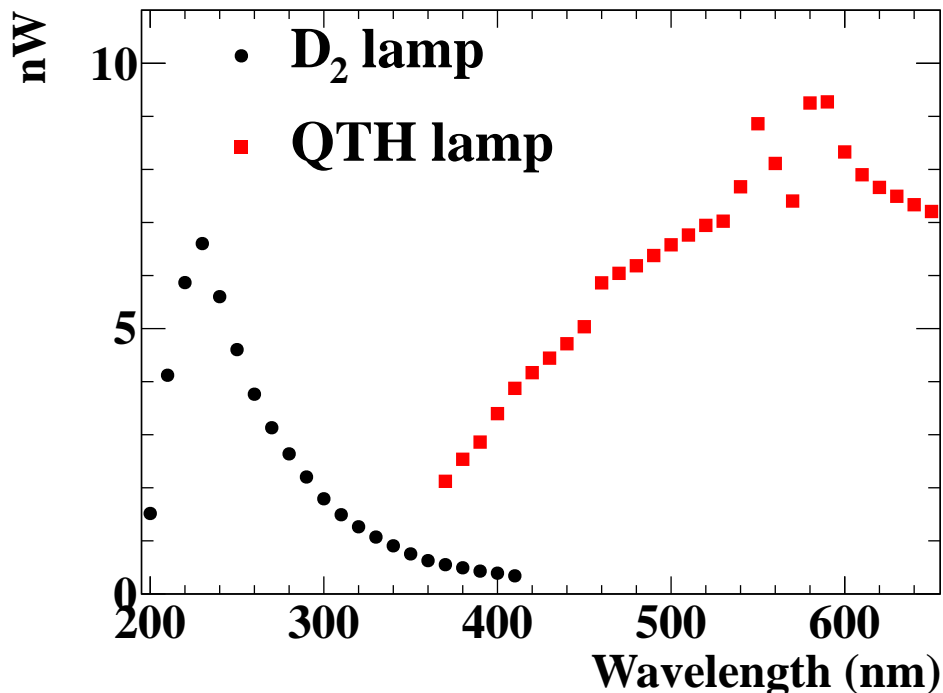


Figure 18: Measured optical power output of the monochromator for the deuterium (D_2) and halogen (QTH) lamps, *not including reflection/absorption in beam splitters and fused silica lenses*. The curves shown represent the sum of the reflected and transmitted optical power through a beam splitter. UV fused silica lenses in front of both photodiodes focus the light onto the detector surface.

of the spot from the center hole can be easily seen, simplifying each alignment operation. To align the lens tube to the correct beam position and direction, two discs were used, one at each end of each lens tube, and the position and orientation of the lens tube were adjusted until the beam passed through both center holes, as shown in Fig. 20.

2.6 Beam splitters

Two beam splitters were used to split the test beam during the reflectivity measurement. For UV measurements using the D_2 lamp, a Thorlabs' model BSW20 non-polarizing plate beam splitter was used. This beam splitter consists of a 1"-diameter, 5 mm-thick fused silica substrate with a beam splitter coating on the front surface optimized for an approximately 50:50 split ratio at 45° angle-of-incidence (AOI) from 250-450 nm and an anti-reflection coating on the back surface. The back surface also has a 30 arc-minute wedge so that the

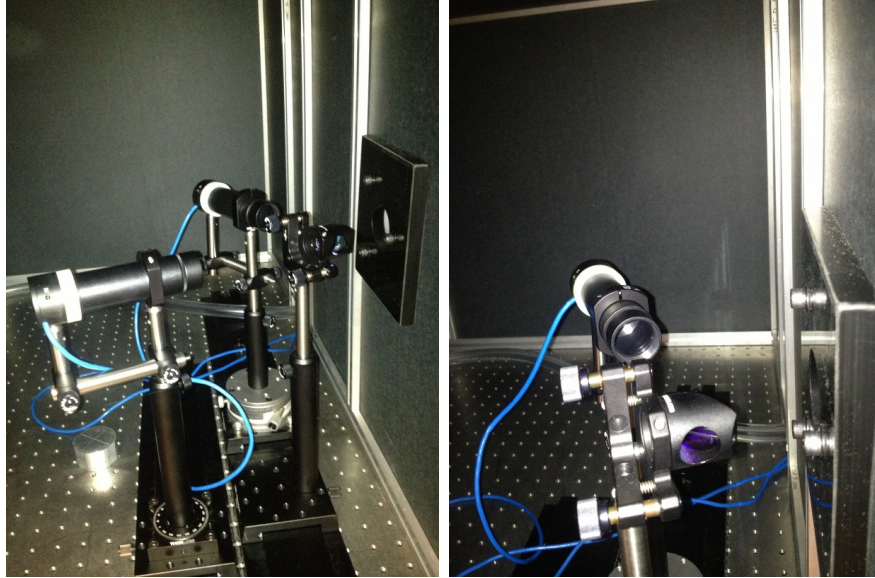


Figure 19: Left: Photodiodes with focusing lens assemblies during a beam splitter calibration measurement. Right: Close-up view of the UV beam splitter and the lens mounted in front of the photodiode. See text for details.

light reflected from the back surface will diverge. For visible light measurements using the QTH lamp, a Thorlabs' model BSW10 beam splitter was used, which is identical to the BSW20 in every respect except that the beam splitter coating is optimized for the 400-700 nm wavelength range. The beam splitters were mounted using the hardware shown in Fig. 19, which includes a kinematic mount with two-axis fine tilt adjustment, a height-adjustable mounting post, and translation along one horizontal direction via a rail carrier. The beam splitters were aligned for 45° AOI with respect to the incident beam according to the procedure described below in section 3.2. The beam splitter reflection/transmission ratio was measured every time the configuration of the beam splitter was changed. The procedure for calibration of the beam splitter is described below in section 3.3. Configuration changes include either changing from the UV to the visible beam splitter or changing the alignment of the beam splitter in any way. Because the beam splitter reflection/transmission ratio is very sensitive to the AOI of the incident beam as well as its polarization, calibration measurements were necessary after every configuration change in order to minimize systematic errors in the reflectivity measurement. Because of the wedged back surface of the beam splitter, the orientation of the beam splitter's front surface is generally not repeatable after removing it from the mount. For this reason, even if the alignment of the mount is not changed, the beam splitters cannot be exchanged without re-calibrating.

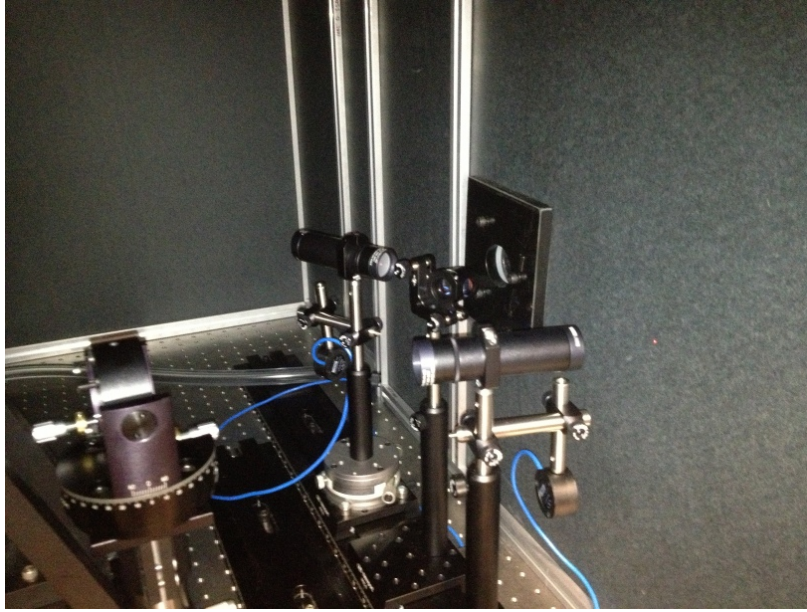
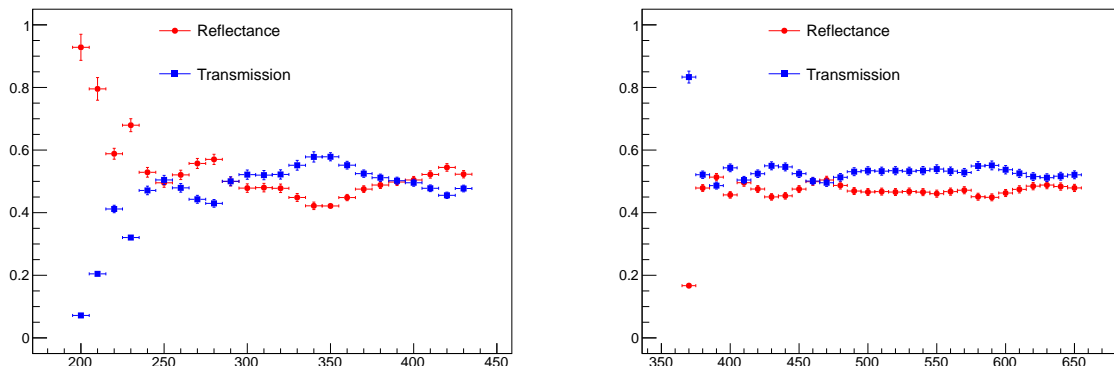


Figure 20: Alignment of the lens tubes using the frosted glass discs with 1 mm through-holes. During alignment, the photodiodes are removed from the beam path, the discs are attached to both ends of each lens tube, and the position and orientation are adjusted until the beam goes through the center holes of both discs.

Figure 21 shows typical examples of measured reflectance and transmission curves for both beam splitters. The relevant quantity for mirror testing is the ratio of reflectance to transmission. For a given beam splitter, this ratio has been found to vary by as much as 5-10% from one calibration to the next, reflecting the high sensitivity of the beam splitter calibration to alignment, positioning, AOI and other variables. As long as the alignment of the lamp, the mirror in the illuminator housing, the beam splitter itself and the photodiode that views the light reflected by the beam splitter remain unchanged between the calibration measurement and the reflectivity measurement, the reflectance/transmission properties do not change and the reflectivity results can be considered reliable.

2.7 Control Mirror

A Newport model 10Z40AL.2 flat broadband metallic mirror was used to perform various alignment activities and as a repeatable reference standard for reflectance measurements. The mirror consists of a UV-enhanced aluminum coating on a 6 mm-thick, 1"-diameter Zerodur substrate, with a protective overcoat of UV-transparent magnesium fluoride to prevent oxidation. The mirror is flat to within $\lambda/20$ at 632.8 nm. Figure 22 shows the "typical" re-



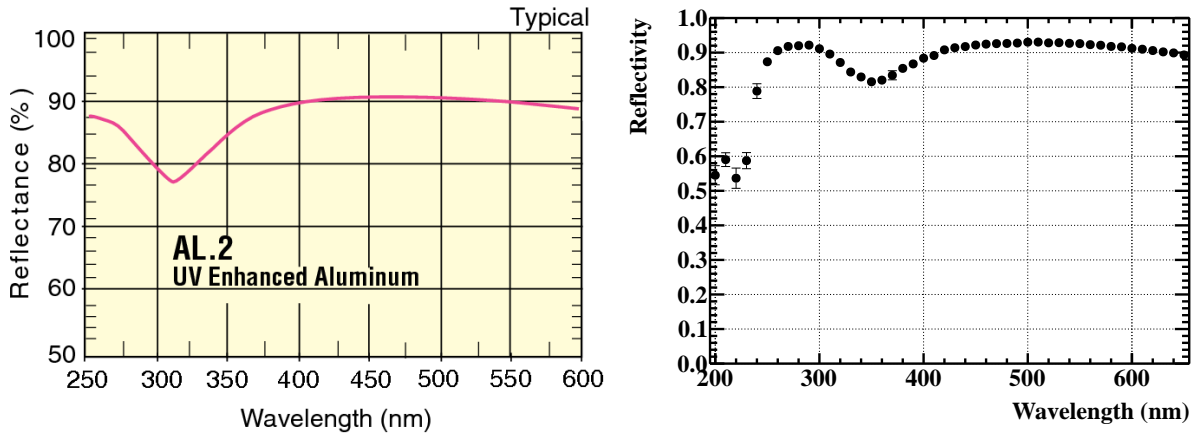
(a) UV beam splitter BSW20 measured reflectance and transmission curves as a function of wavelength in nm. (b) Visible beam splitter BSW10 measured reflectance and transmission curves as a function of wavelength in nm.

Figure 21: Example beam splitter calibration results. “Reflectance” in this context is defined as $R = P_R/(P_R + P_T)$ where P_R and P_T are the reflected and transmitted power, respectively. Absorption and reflection by the beam splitters and focusing lenses is neglected. “Transmission” is defined as $T = 1 - R$. The uncertainties on the data represent the uncertainties in detector calibration, uniformity and linearity added in quadrature.

reflectivity curve for this type of mirror specified by the manufacturer, compared to the results of measurements carried out at JLab on 5/9/2013, according to the procedures described below in section 3. The D₂ lamp was used to measure the mirror reflectance for predominantly UV wavelengths from 200-400 nm, while the QTH lamp was used to measure the reflectance for predominantly visible wavelengths from 370-650 nm. In all cases, the wavelength was scanned in 10 nm increments appropriate for the ~5 nm bandpass of the monochromator as configured. The overlap region between the ranges covered by the two lamps provides a consistency check between measurements obtained using different lamp and beam splitter configurations. In Fig. 22, measurements at five different angles of incidence were performed for both UV and visible wavelength ranges. The data points represent the average of all measurements in the 10 nm interval², while the “error bars” represent the *rms* deviation from the mean.

The smallness of the variations in the results across many different measurements of the same mirror in the same location imply that the actual mirror reflectivity does not depend significantly on the angle of incidence (as expected for a metallic reflector), and

²There were five measurements at each wavelength from 200-360 nm and 410-650 nm, and ten measurements from 370-400 nm.



(a) Typical mirror reflectivity specified by Newport (b) Mirror reflectivity as measured at JLab

Figure 22: Comparison of “typical” mirror performance specified by Newport and reflectance measured at JLab on May 9, 2013. See text for details.

that the measurement technique has small systematic uncertainties, which are estimated at approximately 1-2%.

3 Mirror Test Procedures

This section describes the principles of the measurement and the procedures involved. It does not provide detailed instructions as to how to perform each step mechanically, which requires hands-on training from a system expert.

3.1 Preliminaries and principles of measurement

In order to run the tests, the minimum steps, regardless of what type of test is being performed, are to turn on the lamp or lamps appropriate to the range of wavelengths being scanned, turn on the photodiode picoammeters, connect the monochromator to the PC using the USB cable, power on the monochromator and launch the control software. Once these steps are performed, the subsequent procedures depend on whether one is testing coated HTCC mirror substrates, Winston Cones, the control mirror or other small disc-mounted mirror samples.

Figure 23 shows schematically the principle of the beam splitter calibration and reflectivity measurements. Each reflectivity measurement must be associated with a set of calibration data in order to extract the reflectivity from the measured photocurrents. Denoting the in-

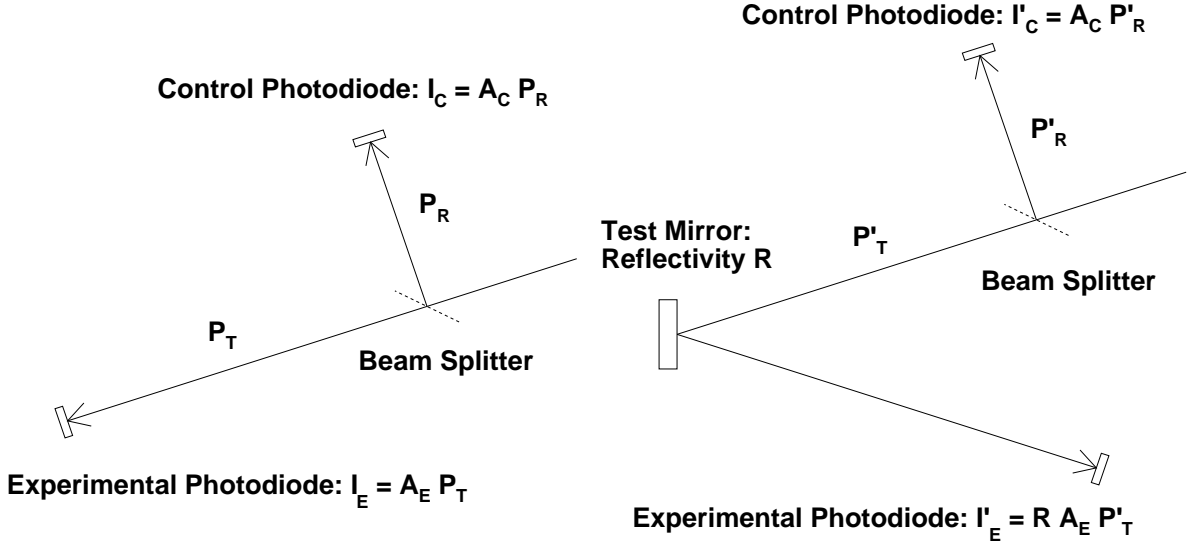


Figure 23: Schematic of beam splitter calibration measurement (left) and mirror reflectivity measurement (right). In the beam splitter calibration, the ratio $\frac{I_E}{I_C} = \frac{A_E P_T}{A_C P_R}$, where A_E and A_C are the responsivities of the respective photodiodes, and $P_R(P_T)$ is the optical power reflected (transmitted) by the beam splitter, respectively. In the reflectivity measurement, the ratio of currents is given by $\frac{I'_E}{I'_C} = \frac{R A_E P'_T}{A_C P'_R}$. Because the reflection/transmission ratio of the beam splitter does not change between calibration and reflectivity measurements, the ratio $\frac{P'_T}{P'_R} = \frac{P_T}{P_R}$. Therefore, the ratio of ratios $\frac{I'_E I_C}{I'_C I_E} = \frac{R A_E P'_T A_C P_R}{A_E P_T A_C P'_R} = R$, independent of the detector responsivities and any differences in incident optical power between the calibration and reflectivity measurements.

incident optical power during the calibration measurement as P_I , the “Control” photodiode measures the power $P_R = R_S P_I$ reflected by the beam splitter, where R_S is the reflectivity of the beam splitter coating. The measured current is $I_C = A_C R_S P_I$, where A_C is the responsivity of the photodiode. The “Experimental” photodiode measures the power $P_T = T_S P_I$ transmitted through the beam splitter, where T_S is the transmission of the beam splitter coating and fused silica substrate (not shown in the figure). The measured current is $I_E = A_E T_S P_I$, where A_E is the photodiode responsivity. The ratio of currents in the calibration measurement is given by:

$$\frac{I_E}{I_C} = \frac{A_E T_S P_I}{A_C R_S P_I} = \frac{A_E T_S}{A_C R_S} \quad (1)$$

Note that the incident power cancels from the ratio. Note also that the ratio T_S/R_S is an intrinsic property of the beam splitter that doesn’t change between the calibration and

reflectivity measurements, provided the alignment of the components is unchanged. Finally, note that the ratio of responsivities $\frac{A_E}{A_C}$ is constant provided the same detectors are used in the respective roles of “Control” and “Experimental” in both measurements.

In the reflectivity measurement, the incident power is P'_I . The current measured by the “Control” photodiode is $I'_C = A_C R_S P'_I$, while the current measured by the “Experimental” photodiode is $I'_E = R A_E T_S P'_I$, where R is the reflectivity of the test mirror. We have implicitly assumed that the incident power is in the linear region of both photodiodes in both measurements, which is a very good assumption for these tests. The ratio of currents in the reflectivity measurement is given by:

$$\frac{I'_E}{I'_C} = R \frac{A_E T_S P'_I}{A_C R_S P'_I} = R \frac{A_E}{A_C} \frac{T_S}{R_S} \quad (2)$$

Comparing equations (1) and (2), we see that the ratio of current ratios gives the mirror reflectivity, independent of the photodiode responsivities, the incident power, or the beam splitter reflection/transmission ratio:

$$\left(\frac{I'_E}{I'_C} \right) \bigg/ \left(\frac{I_E}{I_C} \right) = R \quad (3)$$

This makes the systematic uncertainties of the method rather small.

3.2 Alignment of the beam splitter for 45° AOI using the control mirror

The coatings of the beam splitters described in section 2.6 are optimized for a 45° AOI. Thus it is desirable to align the beam splitter at an angle corresponding as closely as possible to 45° AOI relative to the beam emerging from the collimator. The procedure for doing so makes use of the flat control mirror of section 2.7 mounted in a Newport model 605-2 precision gimbal mount capable of reading the yaw angle using the engraved Vernier scale with 10 arc-minute resolution, and the detector lens tube with alignment discs mounted on the center of a Newport model UTR80 rotation platform, which has a Vernier scale with 1 arc-minute resolution. Although the absolute angles of the mounting hardware relative to the table are not precisely determined, the angle relative to the beam can be determined with rather high (10 arc-minute) precision, limited by the resolution of the gimbal. However, the direction of the laser beam in any given alignment procedure has an inherent uncertainty of a few tenths of a degree relative to the central axis of the collimator due to the finite angular acceptance of the collimator, limiting the overall accuracy of the alignment.

Figure 24 illustrates the geometry involved in the alignment. The steps in the procedure are as follows:

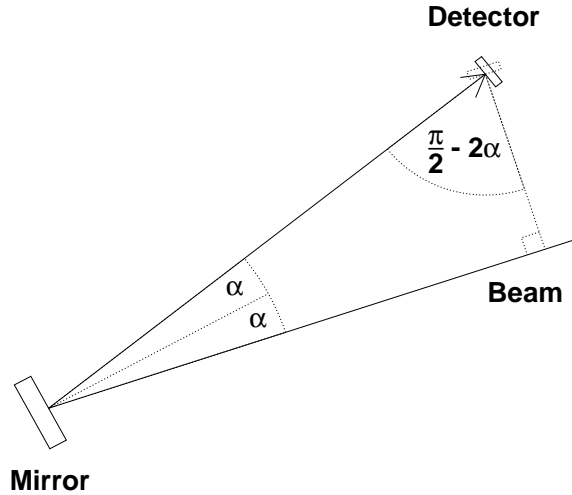


Figure 24: Geometry of beam splitter alignment using flat control mirror. See text for details.

1. The control mirror is rotated in the gimbal until it reflects the laser beam back along its incident direction, and the gimbal angle is recorded. This determines the “zero” of the gimbal angle reading relative to the laser beam.
2. The control mirror is then rotated until the beam is reflected to the approximate desired position of the detector viewing the light reflected by the beam splitter, hereafter referred to as the “control photodiode”.
3. The axis of the lens tube of the control photodiode is aligned with the direction of the beam reflected by the control mirror, and then the angle of the UTR80 rotation platform is recorded. This determines the “zero” of the UTR-80 angle reading relative to the beam reflected by the control mirror.
4. The change in angle of the gimbal after rotation of the control mirror is equal to the angle of incidence α in the triangle shown in Fig. 24. The angle of reflection of the beam by the control mirror is 2α .
5. After determining α (which can be chosen arbitrarily) as in Fig. 24 and aligning the control photodiode at normal incidence to the beam reflected by the control mirror, the control photodiode is then rotated through an angle $\pi/2 - 2\alpha$ to a final orientation perpendicular to the beam, so that it views light reflected by 90° at normal incidence.

6. With the position of the beam splitter fixed so that the beam goes through its center and passes through the apertures of its mounting hardware, and the orientation of the detector fixed so that it is perpendicular to the incident beam, adjustments are made to the orientation of the beam splitter and the position of the detector until the beam reflected by the beam splitter is aligned with the axis of the detector lens tube. This procedure guarantees the alignment of the beam splitter at a 45° AOI relative to the incident beam, to within the accuracy of the laser-collimator alignment.

It is worth recalling that 45° AOI is not strictly required to perform a good measurement, but it is the optimal starting point. Small deviations from this alignment are acceptable as long as a calibration measurement is taken after every and any change in alignment of the beam splitter and/or the control photodiode. Provided the orientation of the control photodiode does not change, the beam splitter can be re-aligned (after exchanging the UV and visible beam splitters, for instance) by simply using the angular adjustments on the beam splitter mount and/or translating the control photodiode to align the reflected beam with the axis of the control photodiode's lens tube, which should already be perpendicular to the beam direction.

3.3 Calibration of the beam splitter

After the beam splitter is aligned, the next step is to take beam splitter calibration data. The goal of the measurement is to determine the reflection-transmission ratio of the beam splitter in its current alignment; i.e., the ratio $\frac{R_S}{T_S}$. First, the experimental photodiode is aligned parallel to the component of the laser beam transmitted through the beam splitter. Then, the laser is turned off, and both photodiodes are secured in place at the end of their respective lens tubes. After closing the black box, the monochromator wavelength is scanned in 10 nm increments across the useful range of the beam splitter in question; 200-400 nm for the D_2 lamp or 370-650 nm for the QTH lamp. In the typical scan, the software configures the monochromator to pause for 7-10 seconds at each wavelength. This provides sufficient time for the current to settle at the new wavelength and for the operator to record both currents before moving to the next wavelength. After completing the scan, the data are saved for later use. An Excel template for data collection is available at [3].

3.4 Measuring reflectivity

The procedure for mounting, aligning and measuring the reflectivity of the test specimen depends on what type of mirror is being tested. The most common examples are described here.

3.4.1 HTCC mirrors

First, the location pins are inserted in the correct hole pattern for the facet being tested (see Figs. 13-14). Gloves are always worn when handling coated HTCC mirror facets, with no exceptions. With the pump off, the mirror is gently held in place against the fixture without touching the reflective surface, using the location pins as alignment guides. When the mirror is ready for the application of vacuum, the pump is turned on. The mirror is then held against the fixture by the differential pressure between the vacuum pump and the surrounding atmosphere. The platform supporting the mirror vacuum fixture is bolted to the table in the desired position and rotated to the desired orientation. The translation stage micrometers can be used for fine positional adjustments, but typically the translation stage position is centered with respect to the rotation platform in order to simplify the calculation of the angle of incidence. The final position and orientation angle of the platform are then recorded for later analysis.

After the position and orientation of the mirror mounting platform are fixed, the experimental photodiode is aligned with the beam reflected by the mirror. For mirrors 2, 3, and 4, this is done in the usual way by translating and rotating the lens tube with alignment discs attached until the beam goes through both center holes. This is possible because the mirror vacuum fixture was designed so that the mirror's central symmetry line lies in a horizontal plane at beam height above the table. When the mirror center line and the incident beam are in a horizontal plane, the plane of incidence and the reflected beam are horizontal at any angle of incidence. For mirror 1 left (right) on the other hand, the half-sector center line is rotated upward (downward) with respect to the horizontal, so that the plane of incidence is tilted slightly downward (upward) by an angle that depends slightly on the orientation angle of the mirror fixture. In this case, the reflected beam has a small but non-zero vertical slope. Since the lens tube cannot be tilted vertically on the existing mounting hardware, the beam in this case impinges on the focusing lens at an angle that is not parallel to the axis of the lens tube, meaning it is not generally possible to align the beam to go through the center holes of both alignment discs. Instead, if the beam is centered on the front alignment disc, it will be displaced vertically at the second alignment disc due to its vertical slope, as illustrated in the left-bottom panel of Fig. 27. In the case of mirror 1, the best practice is to align the lens tube so that the beam goes through the center hole of the first alignment disc and is centered horizontally at the second alignment disc, minimizing the beam offset from the center of the photodiode. As shown by the ray-tracing simulations described below, 100% light collection efficiency is still realized at typical angles of incidence, despite the roughly 2 mm vertical offset of the focused beam spot from the photodiode center. After alignment, the laser is turned off, the alignment discs are removed, and the photodiode is secured in place. Then, the black box is closed and the monochromator wavelength is scanned across the useful range of the lamp/beamsplitter combination currently in use. As is common to all

types of mirror tests, the currents in both photodiodes are recorded and then the reflectivity is calculated from the double-ratio of currents using eqn. (3).

3.4.2 Disc-mounted flat mirrors

For flat mirrors mounted on 1"-diameter discs, such as the control mirror, the Newport model 605-2 precision gimbal mount is used. After securing the mirror in the gimbal, the gimbal is attached to an adjustable-height 2"-square mounting platform clamped to a 1.5"-diameter steel mounting post fixed on the translation stage opposite the mirror vacuum fixture, as shown in Fig. 15(b). The position of the control mirror is adjusted using a) the translation stage micrometers, b) rotation of the UTR160 or c) moving the entire platform (most difficult) until the laser beam is roughly centered on the control mirror. Then, the gimbal rotational adjustments are used to set the desired orientation of the mirror. Finally, as in all tests, the experimental photodiode is aligned to the reflected beam, the laser is turned off and the measurements are performed.

3.4.3 Winston Cones

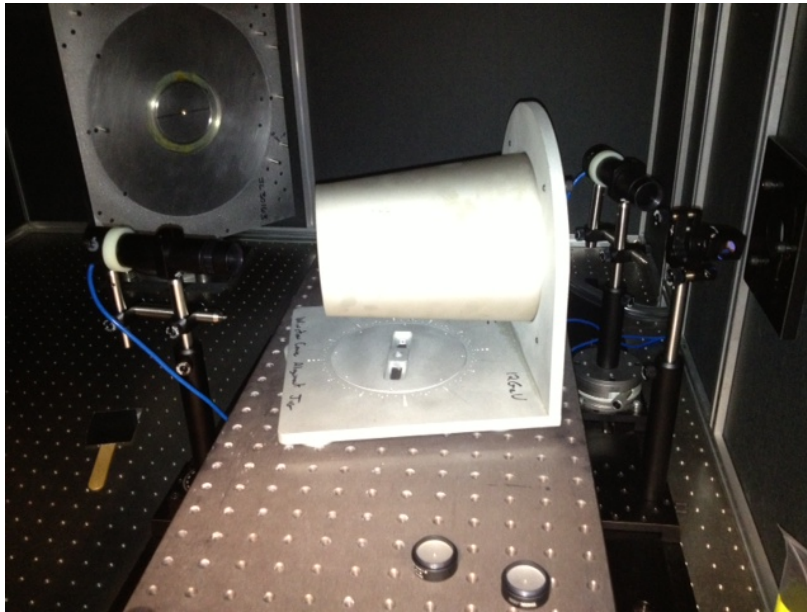


Figure 25: Winston Cone test setup illustrating the Winston Cone mounting fixture. In this example, 3/8"-thick nylon spacers were used to increase the height of the mounting fixture. More typically, the mounting fixture was flat on the elevated breadboard, and leveling feet were used to adjust the height of the breadboard. See text for details.

A custom mounting fixture for the Winston Cones was fabricated at JLab. It consists of a flat base with a circular opening surrounded by coarse angular markings every 6° . A slotted circular disc fits in the opening, allowing for rotation and translation of the base. A single bolt is used to fix the base to a breadboard, as shown in Fig. 25. A vertical mounting frame is attached to the base. It has a large hole through which the Winston Cone fits and four mounting holes aligned with the outer bolt circle on the mounting flange of the Winston Cone itself. Figure 25 shows a Winston Cone mounted in a typical test. A “table” consisting of a small optical breadboard with four legs attached was used to position the Winston cone at the same beam height used for HTCC mirror testing. Leveling feet attached to the legs of the “mini-table” were adjusted until the center line of the cone was at beam height, as determined by observing the vertical slope of the beam reflected by the cone. Although the angle of incidence was not precisely measured in the Winston Cone tests, most of the tests were carried out with the cone’s symmetry axis approximately parallel to the test beam. In this case, the angle of incidence is very large, and the reflection grazing.

The motivation for this test method is two-fold. First, the situation is very close to the situation in CLAS12; the rays collected by the Winston cones in the HTCC are approximately parallel to the axis of the Winston cone. Second, the parabolic geometry of the Winston cone collects incident rays parallel to the axis at a common focal point approximately nine inches behind the back edge of the cone. This focusing property is beneficial to obtaining 100% light collection efficiency for the typically longer path lengths involved in testing the Winston Cones, which pose difficulty even with the focusing lenses in place. As shown in Fig. 25, the experimental photodiode is positioned behind the Winston cone, viewing a grazing reflection off the side of the reflected surface.

3.5 Simulation

To calculate the AOI and the light collection efficiency in each measurement, a ray-tracing Monte Carlo simulation of the setup was designed using the ROOT libraries. Rays are generated with uniform distributions in $\cos\theta$ for $0 \leq \theta \leq 1^\circ$ and in ϕ for $0 \leq \phi \leq 2\pi$, where θ and ϕ are, respectively, the polar and azimuthal angles of the generated rays relative to the central axis of the collimator³. The initial coordinates of the rays are generated with a uniform transverse spatial distribution in the plane perpendicular to the central axis of the collimator at a point 20 mm upstream of the first pinhole aperture of the collimator, for radii less than 0.8 mm^4 . Each ray is then projected to the first and second apertures of the collimator. Rays with radial displacements from the axis exceeding the hole radius

³Although the monochromator acceptance cone has a half-angle of 7.4° , the upper limit for the generation of θ is set to 1° to increase the efficiency of the simulation, since this is sufficient to populate the full acceptance of the collimator.

⁴This generation limit for the radius is the minimum initial beam size needed to populate the full angular and spatial acceptance of the collimator.

at either aperture are rejected. Rays passing through both pinholes are then projected to their intersection point with the surface of the mirror, where the AOI and the direction of the reflected rays are calculated. The reflected rays are then projected to the surface of the lens, and traced through the lens using Snell's law together with the known geometry and index of refraction of the lens and the surrounding air. Reflection and absorption by the fused silica lens are neglected; i.e., 100% transmission is assumed. Finally, the refracted rays transmitted through the lens are projected to the surface of the photodiode, where their position and angles relative to the detector center are calculated.

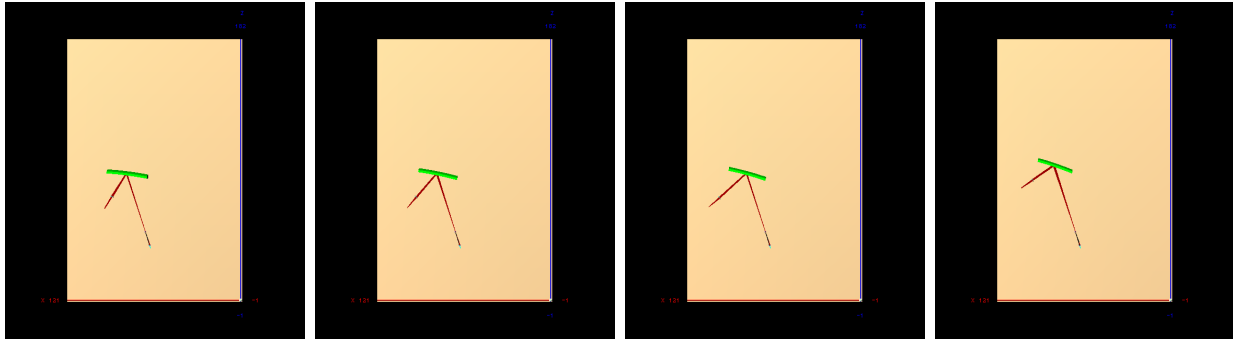


Figure 26: View from above the table of the ray-tracing simulation for mirrors 1 left, 2, 3 and 4 from left to right. In each case, the position and orientation of the mirror were chosen so that the AOI of the test corresponds to the central AOI for rays originating from the target in CLAS12.

Figure 26 displays the simulation results of four different reflectance tests, as seen from above the table. The position and orientation of the platform in each test were chosen so that the central AOI of the reflectance test corresponds to the value given in Table 1 for the central θ of the mirror facet being tested. The path lengths shown are typical of real tests. Figure 27 shows the resulting distribution of the reflected rays at the photodiode surface for each of the four tests for two different cases. In the first case, the reflected rays are projected directly to the photodiode surface, without any focusing lens. In the second case, the reflected rays are traced through the focusing lens using Snell's law and the known geometry of the lens.

In the first case, the collection efficiency is close to 100%, assuming perfect alignment of the experimental photodiode with respect to the central ray. In actual tests, however, small offsets of the actual detector position from the center of the reflected beam spot are possible due to the uncertainty in the laser-collimator alignment. The simulation results clearly show that without the focusing lens, alignment errors as small as one to several mm can lead to significant light losses, because the size of the reflected beam spot is comparable to the size of the photodiode surface. Since the alignment error in any given measurement

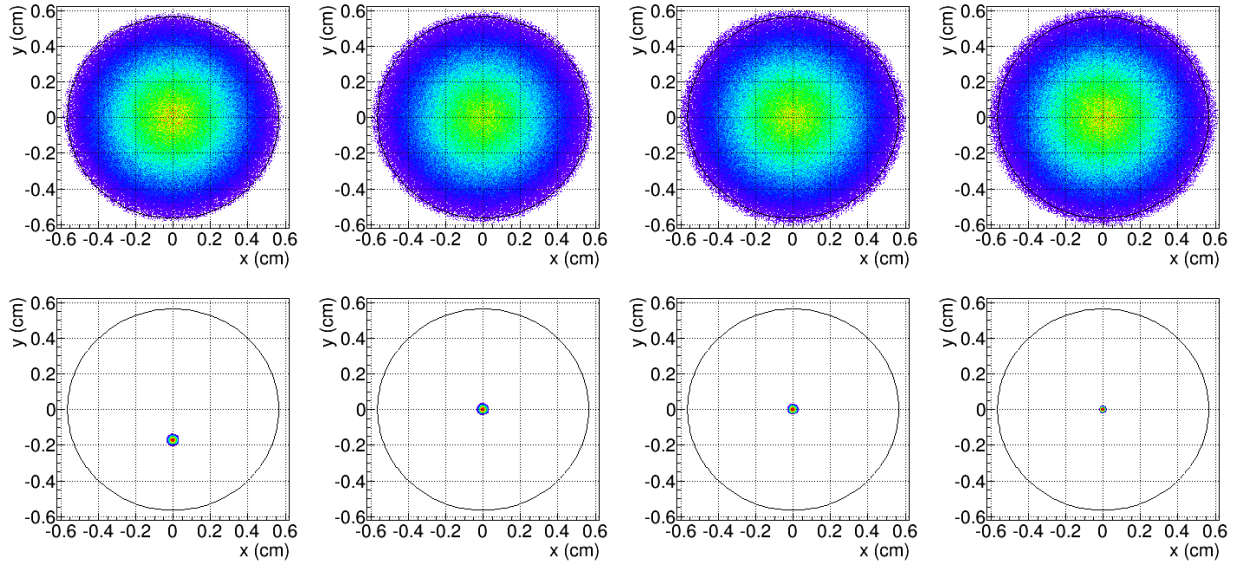


Figure 27: Distribution of rays at the detector surface corresponding to the tests shown in Fig. 26, for mirrors 1 left, 2, 3 and 4 from left to right. The top (bottom) panel in each column shows the distribution of rays at the detector surface without (with) the focusing lens. The drawn circle shows the radius of the photodiode active area. Assuming perfect alignment of the test, the collection efficiencies without the lens in the four tests are 99.8%, 99.7%, 99.3% and 99.2%, respectively. Because the beam spot size is comparable to the photodiode diameter, even slight misalignments can significantly reduce the collection efficiency in this case. With the focusing lens, on the other hand, the collection efficiency is 100% in all cases, even in the case of mirror 1 left, for which the vertical slope of the reflected rays displaces the focus vertically by roughly 2 mm.

is unknown, the resulting collection inefficiency is also unknown and cannot be determined, except via a time-consuming process of locating the true center of the reflected beam spot by intentionally offsetting the detector position in both directions relative to the position determined via laser alignment. Since it is not practical to determine the true beam center in every test, unknown collection inefficiencies introduce systematic error and bias (toward lower reflectivity values) in the test results.

In contrast, the optics of the measurement with the focusing lens are much more forgiving. Even in the case of mirror 1, where the vertical slope of the reflected beam induces a roughly 2 mm vertical displacement of the focused beam spot at the detector, alignment errors can be as large as 2-4 mm and the collection efficiency is still 100%. The focusing lens, by increasing the effective light collection area of the photodiode by roughly a factor of four, drastically

reduces the sensitivity of the results to alignment errors.

3.6 Angular calibrations

In the simulation of any given measurement, the position and orientation of each mirror relative to the optical table are calculated from the known position of the UTR160 relative to the optical table and the known orientation angle of the UTR160. The drawings shown in Figs. 13-14 show the positions of the ellipse focal points relative to the central pivot point of the UTR160 for a nominal, arbitrarily chosen orientation angle of the UTR160 relative to the table. From these drawings, one can calculate the focal point positions for any position and orientation of the UTR160, assuming the mirror facet conforms to its design geometry and its positioning on the vacuum fixture using the location pins is exact.

The position and orientation of the collimator are calculated from the monochromator design drawings and manual measurements of the monochromator as it exists on the optical table. The nominal angle of the beam/collimator axis relative to the table is 18.3° ; it can be measured with very good accuracy by reflecting the beam off the control mirror toward a distant target mounted at a known position on the table. Given the known positions of both the control mirror and the target, the angle can be triangulated very precisely, limited only by the resolution of the vernier scale on the gimbal mount. Moreover, once the beam/collimator angle relative to the table is determined, the known position of the beam at the control mirror can be used to calibrate the position of the collimator itself. A recent measurement found that the collimator angle was 17.83° [3], compared to a nominal value of 18.29° . Notably, the position of the collimator predicted using the measured beam angle and the known position of the control mirror agrees with its nominal value to within 1 mm, whereas the projected position using the nominal beam angle substantially disagrees with the nominal position.

Because the UTR160 is attached to its baseplate at an arbitrary orientation angle using clamping bridles, its absolute orientation relative to the optical table is not *a priori* known, but instead must be calibrated with respect to other “known” quantities. There are several methods for determining this angle. In one such method, the UTR160 is mounted in a known position with an HTCC mirror facet attached to the vacuum fixture. Then, it is rotated until the mirror reflects the beam back along its incident direction, and the angle of the pivot is recorded. This angle is then compared to the predicted pivot angle for which the back-reflection condition occurs to determine the offset between the angular scale of the UTR160 and the angle of the pivot measured in the table coordinate system. The main weaknesses of this method are its reliance on the assumption that the mirror geometry and positioning conform exactly to their design values and the inexact knowledge of the collimator position and angle relative to the optical table.

Calibration of the UTR160 angle using the control mirror is complicated by the fact that the absolute orientation of the gimbal mount relative to the UTR160 is unknown, because

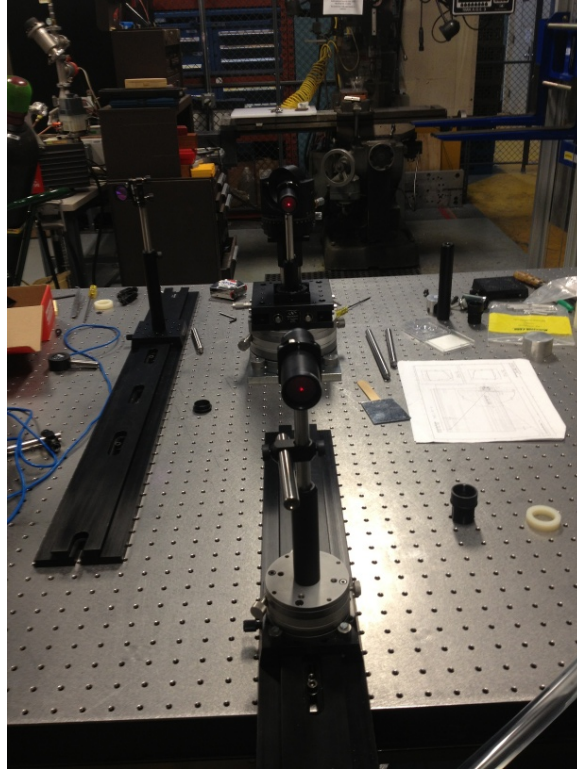


Figure 28: Alignment of the UTR160 platform with respect to the optical table. See text for details.

the platform on which the gimbal is supported is free to rotate with respect to the 1.5"-diameter steel post onto which it is clamped. In order to calibrate the angular scale of the UTR160 relative to the table, the control mirror was mounted above the hole at one edge of the translation stage along its central row of holes, and a lens tube was mounted along the same row of holes at the opposite side of the stage, as shown in Fig. 28. The lens was removed from the tube so as not to distort the laser beam, and alignment discs were attached to both ends. The tube was post-mounted on its own small rotation platform for easy orientation. The principle of the alignment is to aim the laser beam at the center of the control mirror, and reflect it through the center holes of both alignment discs. This condition can only occur when the reflected beam and the lens tube are directly above and parallel to the central row of holes on the translation stage, since the beam must pass through two points directly above two of these holes.

The orientation of the UTR160, the gimbal mount and the lens tube were adjusted until the condition shown in Fig. 28 was achieved. The laser beam is reflected from the center of the control mirror and is aligned to go through the 1 mm-diameter apertures of four

alignment discs. The first two alignment discs force the beam to be parallel to the central row of holes on the translation stage. The second pair of alignment discs is attached to a second lens tube, which is carried on a rail that runs parallel to the row of holes along which the UTR160 is centered. The second lens tube is mounted at the center of a UTR80 rotation platform that provides rotation about the vertical axis, and is located on the far opposite side of the table from the UTR160. These alignment discs force the beam, and therefore the UTR160, to be parallel to the x -axis of the table coordinate system. Given the size of the holes in the alignment discs and the distance between the two lens tubes, the uncertainty in the alignment of the beam relative to the optical table is estimated to be less than 5 mrad. On the other hand, the uncertainty in the alignment of the UTR160 relative to the beam is larger due to the smaller ratio of path length to aperture size. A conservative estimate of this angular uncertainty is on the order of $\tan \Delta\theta \sim 1 \text{ mm}/75 \text{ mm}$, implying $\Delta\theta \sim 0.8^\circ$. Results of the measurement of the collimator orientation angle and the calibration of the UTR160 angular scale can be found at [3]. These results apply only to the configuration of the hardware that existed in early August, 2013 and must be repeated after any change; e.g., if the UTR160 is detached and then re-attached to its baseplate.

3.7 Test plan

A well-designed program of tests carried out on each mirror involves measurements in the UV and visible regions at 3-5 distinct, well-separated points on the mirror and in a range of angles of incidence corresponding to the typical AOIs for Cherenkov photons emitted by scattered electrons in CLAS12. The main tasks of data analysis are to combine all test results from a given mirror, evaluate the averages and statistical variances of the results, investigate correlations of the results with angle of incidence, the position on the mirror being tested, or any other relevant variable of the tests, and to store the results in a database for long-term storage and future use. The outcome of the testing and analysis of the results is a final decision on acceptance or rejection of the mirror for use in the CLAS12 HTCC. The decision to accept or reject a mirror depends on the expected average signal strength corresponding to the mirror's reflectivity, which is given by a convolution of the measured reflectivity with the PMT quantum efficiency, the spectral distribution of Cherenkov radiation, the transmittance of CO₂ and the light collection efficiency. All but the light collection efficiency are strongly wavelength-dependent. The transmittance of CO₂ is close to 100% from 220-650 nm, but drops quickly to zero below about 190 nm. The (geometric) light collection efficiency is close to 100% for the HTCC optics design. Neglecting the change in velocity of the electron as it traverses the CO₂ gas volume of the HTCC, the expected average number of photoelectrons is given by[2]:

$$\langle N_{pe} \rangle = L \int_{\lambda_1}^{\lambda_2} d\lambda \frac{2\pi\alpha}{\lambda^2} \sin^2 \theta_C(\lambda) \epsilon(\lambda) R(\lambda) (T_{CO_2}(\lambda))^{d/L_{abs}}, \quad (4)$$

Mirror Facet	Scattering angle θ (deg.)	AOI (deg.)	Path length in gas (meters)
1	35.0	24.77	1.57
1	31.25	24.96	1.53
1	27.5	25.03	1.48
2	27.5	29.042	1.48
2	23.75	29.108	1.43
2	20.0	29.037	1.37
3	20.0	33.06	1.37
3	16.25	32.96	1.31
3	12.5	32.73	1.24
4	12.5	36.70	1.24
4	8.75	36.43	1.17
4	5.0	36.03	1.10

Table 1: Angles of incidence and path lengths in CO₂ for rays scattered from the CLAS12 origin at an angle θ relative to the beam direction along the mirror half-sector center line. The path length in this context is defined as the distance from the origin to the intersection of the ray with the mirror center line, minus the distance from the origin to the HTCC entry window at that θ , and represents the path length along which Cherenkov photons are *emitted* by fast electrons.

where L is the path length in the radiating medium, $\theta_C = \cos^{-1}\left(\frac{1}{\beta n}\right)$ is the Cherenkov emission angle, ϵ is the quantum efficiency of the PMT, R is the mirror reflectivity, T_{CO_2} is the transmittance of CO₂ for a fixed path length L_{abs} , and d is the path length traveled by emitted Cherenkov photons. Table 1 shows the angles of incidence and path lengths in CO₂ for rays scattered from the CLAS12 origin for each mirror facet, at scattering angles θ corresponding to the minimum, maximum, and central θ subtended by the mirror along its center line.

The basic testing and data analysis plan for each mirror, then, consists of the following tasks:

1. Run the tests. Ideally, at least five well-separated points on the mirror should be tested in both UV and visible. Positioning and orientation of the mirror are repeatable provided all necessary information is recorded for each scan. The points/angles to test should be chosen according to the following guidelines:
 - For at least one test, the position and orientation of the platform should be chosen so that the beam reflects from a point near the center of the mirror at an AOI corresponding to the central AOI given in table 1. The ROOT macro

`AOI_vs_phi.C` available at [3] can be used to calculate the required orientation angle of the rotation platform corresponding to a desired AOI, given the position of the platform.

- The other tests should occur at points that are spatially well-separated from the point corresponding to the central AOI. While this is most easily accomplished by rotating the platform, test points reached by rotating the platform will have a different AOI. In principle this is not a problem since the theoretical reflectance of the coating varies only weakly with AOI for a metallic reflector coating at typical angles involved in our measurements.
 - If significant non-uniformities in reflectivity are observed when different points are reached by rotating the platform, then one can test whether the underlying cause is an AOI-dependence or a position dependence of the reflectivity by moving the entire platform and re-testing at the central AOI, but at a different position on the mirror.
 - For every scan, all requisite information must be recorded to enable simulation of the test and reconstruction of the AOI and light collection efficiency (see simulation documentation at [3] for required geometric information).
 - Any test for which the simulated light collection efficiency differs substantially from 100% should be discarded.
 - All mirror positions tested in UV should be repeated in visible, and vice versa. The mirror positioning is repeatable, provided all required information is recorded.
2. Generate ROOT graphs of each individual scan using `MirrorTestAnalysis_new.C`.
 3. Simulate each scan to calculate AOI and collection efficiency using `reflectance_test_simulation.C`.
 4. Combine scans from individual mirror tests using `CombineMirrorTests.C`.
 5. Estimate the average signal strength (number of photoelectrons) for the combined reflectance results of each mirror using `calc_signal_strength.C`.

More details of the analysis procedures and all utility programs (compiled ROOT macros) can be found at [3].

4 Results

4.1 Flat test samples

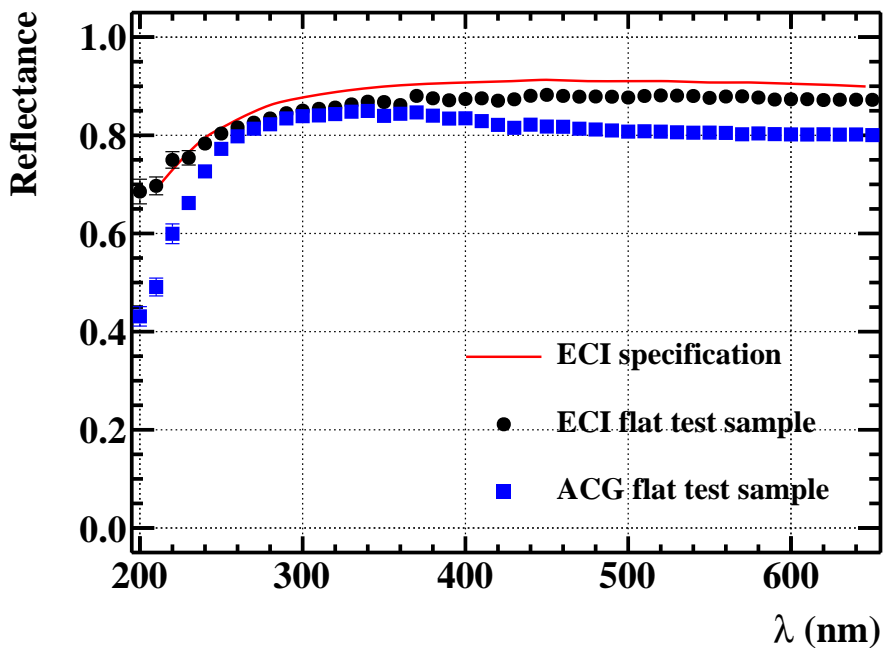


Figure 29: Comparison of reflectivity results for flat acrylic samples, subjected to the same thermal shaping process used for the HTCC mirror front and back faces, and deposited with reflective coating by two different vendors, Applied Coatings Group (ACG) and Evaporated Coatings Incorporated (ECI). The results provided by ECI are superior to those achieved by ACG within the entire wavelength range of interest. The red solid curve shows the theoretical performance specification of the coating provided by ECI.

Flat sheets of acrylic subjected to the same thermal shaping process applied to the front and back surfaces of HTCC mirror facets were shipped to four potential vendor companies, where they were vacuum-deposited with a reflective coating of Aluminum and a protective overcoat consisting of varying UV-transparent materials, including MgF_2 , SiO_2 and others. Figure 29 shows the resulting reflectance of the coatings for the two vendors that achieved the best results. The results achieved by Evaporated Coatings, Incorporated (ECI) are superior to those provided by Applied Coatings Group (ACG) in the entire wavelength range of interest. Whereas ACG used a protective overcoat of quartz, which provides excellent mechanical hardness at the expense of somewhat lower reflectivity, ECI uses a proprietary material. No information about the composition of this material was supplied. ECI has provided a curve representing the “theoretical” coating performance. The actual measured reflectivity of the coating as deposited on the thermally shaped acrylic test samples is slightly below this specification. The difference is attributed in part to surface imperfections introduced by

JLab’s thermal-shaping process. On the basis of the results shown in Fig. 29, the contract for coating of all 60 HTCC mirror facets was awarded to ECI.

4.2 HTCC Mirrors

As of March, 2013, five “production” mirrors for the HTCC had been coated by ECI and tested at JLab. Of these, only one was accepted without reservation, and another was tentatively accepted. The “first article” mirror (Mirror 1 left, #12) showed no obvious visual defects, and its measured reflectance was consistent with the flat sample results. Based on this result, ECI was instructed to coat four additional mirrors, one each of the other four facet geometries. Mirror 3 #10, coated by itself in a single run, was returned with a large stain covering approximately 20% of the area of the mirror. While tested points outside of the stained area exhibited acceptable reflectance, the reflectance of points inside the stain had reflectance at least a factor of two lower, making this mirror unacceptable. Three additional mirrors (1R-12, 4-12 and 2-12) were coated together in the same vacuum chamber. Mirrors 1R-12 and 2-12 exhibited unacceptably low reflectance (at least 10% lower than the flat samples in terms of signal strength). ECI noted that the visual appearance of mirror 1R-12 before coating had been the best of any facet in the first batch of five, and that this mirror was cleaned the least aggressively of any of the first five mirrors before coating, suggesting a correlation between the cleanliness of the surface before coating and the ultimate performance of the coating. Mirror 4-12 had acceptable reflectance, but showed several small scratches and smears, making it potentially unusable. It was also hypothesized that coating several mirrors at the same time in the same vacuum chamber adversely impacted the coating performance due to increased outgassing from the foam substrates, reducing the quality of the vacuum.

JLab personnel including Youri Sharabian and Andrew Puckett visited ECI on May 20, 2013 to discuss all aspects of the mirror manufacturing and coating process and attempt to resolve the various problems. A significant problem discovered after the coating of the first five facets was a residue left by the protective adhesive masking tape applied to the front surface of the mirror to protect the acryl surface during trimming of the facets to their final shape. This residue, if not properly removed from the surface, can interfere with the adhesion and performance of the coating in an unpredictable way. Two additional spare mirrors (of type 3) have been coated so far in order to test improved cleaning and coating procedures designed by ECI. This section presents the results of all mirrors tested so far.

Table 2 summarizes the test results for the first seven HTCC mirror facets coated by ECI in terms of the expected average signal strength corresponding to the measured reflectivity. The uniformity (or lack thereof) of the measured reflectivity across the various points and angles of incidence tested is characterized by σ_R , which is defined as the standard deviation of the ratio of each individual measurement to the average of all measurements of the same mirror at the same wavelength, integrated over all wavelengths. The values of σ_R are typically on

Mirror name	Avg. N_{pe}	σ_R	Ratio	Status
Mirror 1 left, #12	35.54	0.022	0.981	Accepted
Mirror 1 right, #12	31.80	0.023	0.878	Rejected
Mirror 2, #12	30.61	0.017	0.904	Rejected
Mirror 3, #10	29.97	0.013	0.965	Rejected (stain)
Mirror 4, #12	27.42	0.027	0.980	Tentative acceptance (smears/scratches)
Mirror 3, #2 (spare)	31.58	0.006	1.017	N/A
Mirror 3, #8 (spare)	29.98	0.007	0.966	N/A

Table 2: Summary of results of first seven HTCC mirrors coated by ECI. “Avg. N_{pe} ” is the estimated average signal strength corresponding to the measured reflectivity. “ σ_R ” is the standard deviation of the distribution of ratios of individual reflectivity measurements to the average of all measurements at the same wavelength. “Ratio” is the ratio of the estimated signal strength to that obtained from ECI’s flat test sample results. “Status” is the acceptance/rejection status of the mirror, and the reason for the decision, if other than low reflectance.

the order of 1-2%, consistent with the estimated systematic uncertainties of the individual measurements. Measurements taken before the installation of the focusing lenses to aid in light collection typically exhibited more non-uniformity than those obtained using the focusing lenses. This observation suggests that some of the fluctuations observed in earlier measurements result from light collection inefficiencies as opposed to actual non-uniformities of the mirror reflectivity. The “Ratio” presented in Table 2 compares the estimated average signal strength corresponding to the measured reflectivity of the mirror in question to the expectation based on ECI’s flat test sample results. The expected signal strength varies among the four mirror facets due to the difference in path length (see Table 1).

Figure 30 shows the estimated average signal strength corresponding to the measured reflectivity of Mirror 1 left, #12, calculated from equation (4) using the values of PMT quantum efficiency for quartz windows and CO₂ transparency from Fig. 4. The “differential” signal strength is the average number of photoelectrons in the 10-nm wavelength interval centered on each wavelength, while the “integral” signal strength is the average number of photoelectrons integrated from 200 nm to the wavelength in question. Given the range of spectral sensitivity of the PMTs, the cumulative signal strength typically saturates above 600 nm. Figure 30 illustrates the importance of high reflectivity at UV wavelengths, due to the approximate λ^{-2} dependence of the distribution of Cherenkov radiation, as more than half the total signal strength comes from wavelengths below 300 nm.

Figure 31 shows the wavelength dependence of the reflectivity for each of the first seven mirrors coated by ECI, compared to the coating performance specified by ECI. All of the mirrors tested so far have fallen below the specification in the plateau region where the

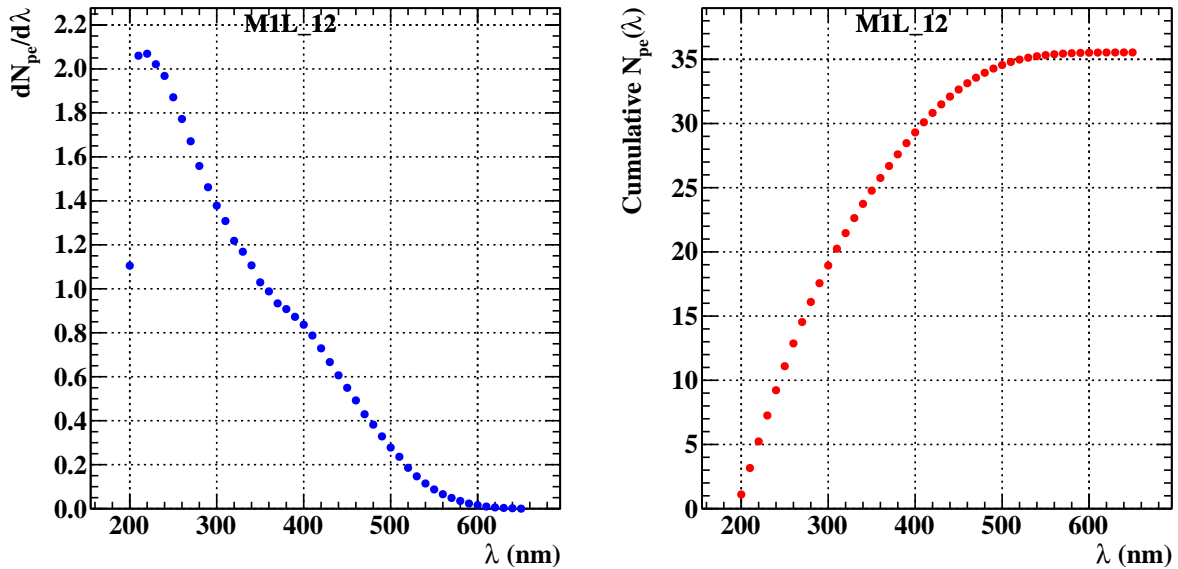


Figure 30: Estimated average signal strength corresponding to the measured reflectivity curve for Mirror 1 left, #12. The left panel shows the “differential” signal strength defined as the average number of photo-electrons in the 10-nm interval centered on that wavelength. The right panel shows the “integral” signal strength defined as the cumulative average number of photoelectrons integrated from 200 nm up to that wavelength; i.e., it is the integral of the left panel.

expected reflectivity is approximately 90-91%. The best results achieved so far for HTCC mirrors are comparable to the results of the flat test samples. One of the two spare mirrors coated to test an improved cleaning process (Mirror 3-2) showed the best performance thus far, exceeding even the specification below 250 nm, while reaching a plateau at about 87%, comparable to the flat sample results. In terms of expected signal strength, the reflectance of this mirror exceeds that of the flat test sample by roughly 2%. The second spare mirror (Mirror 3-8) showed significantly lower reflectance for the same cleaning process. This mirror, which was one of the earliest mirror substrates fabricated at JLab, before the assembly tooling and procedures had been optimized, had a rough and wavy surface quality, in contrast to the very smooth optical-quality surface of the mirrors assembled using the final, optimized tooling and procedures. Even with this poor surface quality, the reflectance achieved using ECI’s new cleaning process was acceptable, corresponding to a signal strength of $\sim 97\%$ of the flat sample benchmark.

To summarize, of the five initial mirror facets coated by ECI, only two met acceptable performance criteria and only one was deemed acceptable “without reservation”. The test

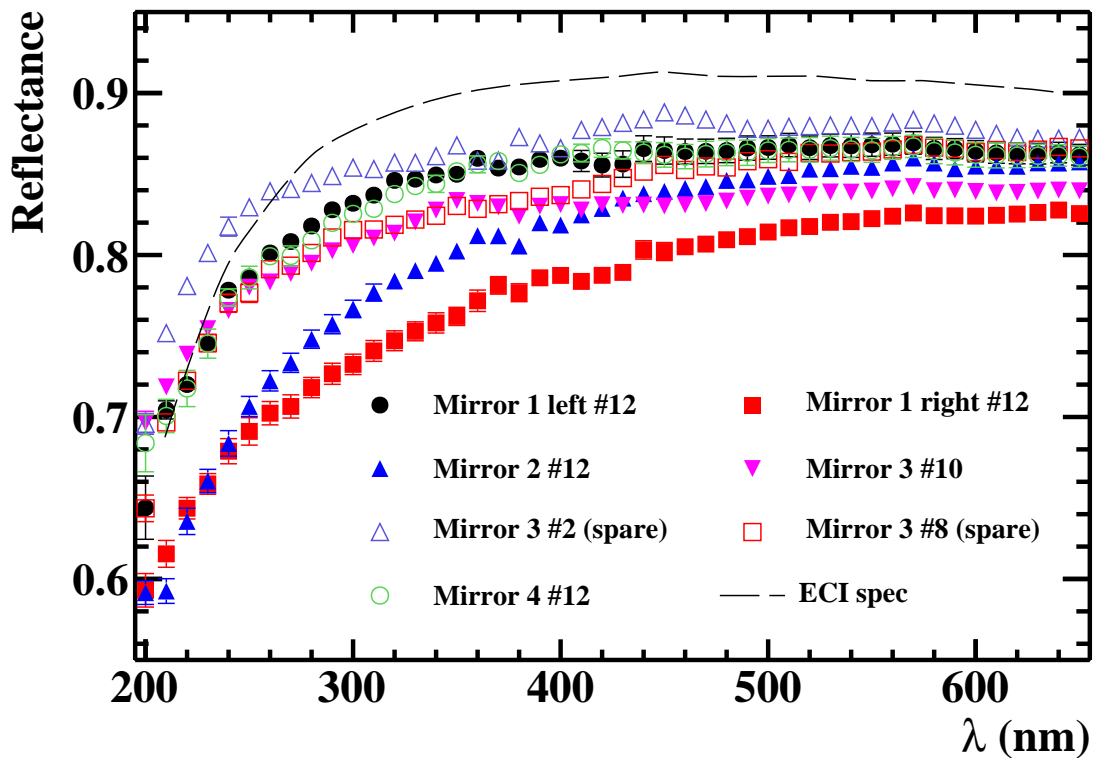


Figure 31: Reflectivity results for the first seven mirrors coated by ECI, compared to the “theoretical” coating performance specification.

results of two additional coating runs performed by ECI on spare mirrors are encouraging and suggest an improved cleaning process will enhance the reliability of the results. No significant AOI or position dependence of the reflectivity has been observed in tests of the HTCC mirrors so far.

4.3 Winston Cones

In contrast to the obstacles encountered in coating the HTCC mirror facets, the coating of the Winston Cones used to increase the light collection efficiency of the HTCC optics from $\sim 80\%$ to nearly 100% has proceeded quickly and with a high success rate. As of this writing, 52 Winston cones have been coated, received and tested. Of these, only four Winston cones exhibiting mechanical defects, poor reflectance, or both have been rejected and are in the process of being rebuilt.

Figure 32 shows the measured reflectance vs. wavelength for the first Winston Cone

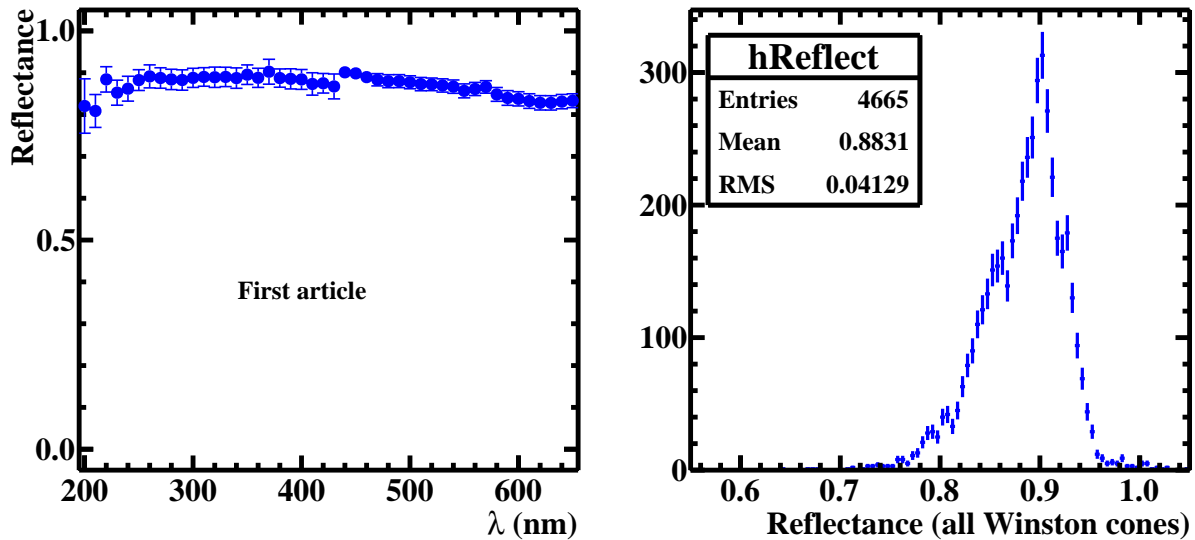


Figure 32: Left: Reflectance vs. wavelength for the “first article” Winston cone coated by ECI. The “discontinuity” at $\lambda = 440$ nm reflects a small systematic difference between measurements taken in the UV and visible regions. Right: The distribution of all reflectance measurements for all 52 Winston Cones received thus far, regardless of wavelength.

coated by ECI, as well as the distribution of all reflectance measurements for all Winston cones. The testing of Winston Cones typically carries a larger systematic uncertainty and the variations in the results reflect this. The angle of incidence and optical path length are generally not repeatable from one test to the next. Moreover, the tests are carried out at large angles of incidence where the reflectivity is not necessarily constant, and at large optical path lengths more susceptible to light collection inefficiencies. For these reasons, larger variations are typically observed among different scans of the same Winston cone than in tests of HTCC mirrors.

All 52 Winston cones coated by ECI so far have been tested in the UV region. Only a small subset of the Winston cones, including the “first article”, were tested in the visible region. Because only $\sim 20\%$ of the Cherenkov light is reflected by the Winston cones, and because most of the emitted Cherenkov light is in the UV region, testing of all Winston cones in the visible region was deemed unnecessary. All mirrors and Winston cones tested in the visible region have shown approximately constant reflectance from 400-650 nm. Figure 33 shows the average reflectance of all Winston Cones tested as a function of wavelength in the UV region. The measured reflectance of the Winston cones is approximately constant from 200-400 nm, with an average value of 88.4%. The generally higher reflectivity of the

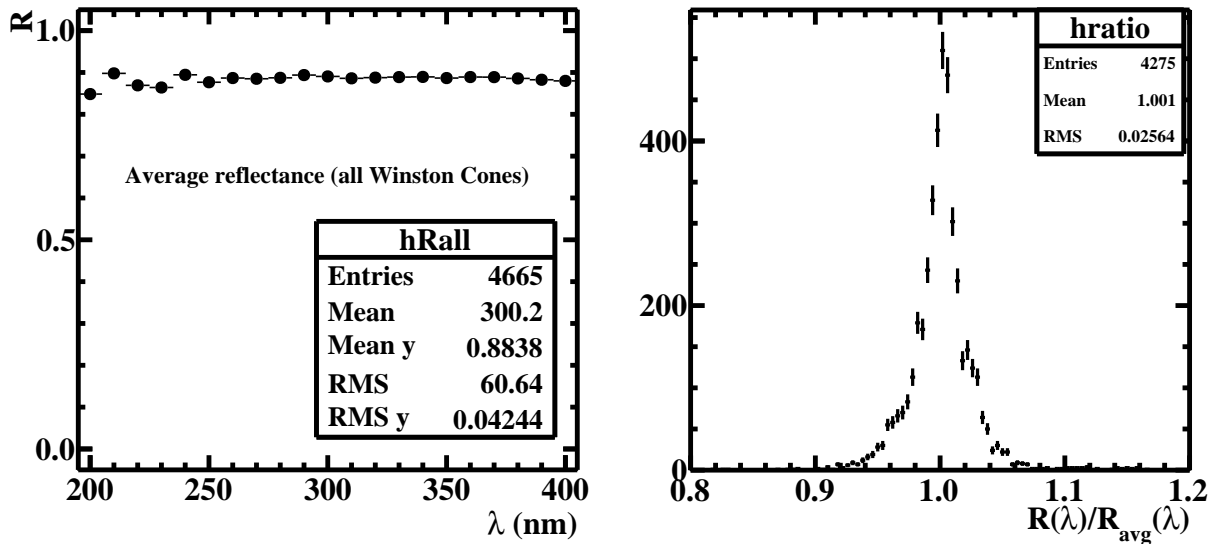


Figure 33: Left: Reflectance vs. wavelength, averaged over all Winston cones, in the UV region. Right: Ratio of individual measurements to the average result at the same wavelength from the same Winston cone, summed over all wavelengths and Winston cones.

Winston cones compared to the HTCC mirrors tested so far reflects the difficulty in achieving a high-quality vacuum deposition onto the mirror facets, with their foam substrates and thermally shaped acryl surfaces, compared to the smooth metallic surface of the Winston cones. The right panel of Fig. 33 shows the distribution of the ratio of individual reflectivity measurements to the average of all measurements of the same Winston cone at the same wavelength, summed over all wavelengths and all Winston cones. The standard deviation of this distribution is about 2.6%, reflecting the larger fluctuations present in measurements of the Winston cones.

To summarize, a total of 52 Winston cones were fabricated, coated by ECI and received at JLab for testing. Of these, four were rejected and returned for repairs or rebuilding. The measured reflectivity of the Winston cones is approximately constant from 200-400 nm and its average value is 88.3%, which meets the performance requirements of the HTCC.

5 Summary and Conclusions

An apparatus has been constructed to measure the reflectivity of the mirrors and Winston cones of the CLAS12 HTCC. This apparatus is capable of measuring the reflectance with small systematic uncertainties of 1-2% and negligible statistical uncertainties. A vacuum-

based mounting fixture allows for repeatable, known positioning of HTCC mirror facets on the test stand without contacting the edges of the mirror or its reflective surface. The mirrors can easily be tested at any AOI within the useful range of angles for CLAS12 at any position along the half-sector center line (for mirrors 2-4) or at any position along a line $\pm 5^\circ$ out-of-plane of the half-sector center line (mirrors 1L, 1R). With additional effort, points at different locations can also be tested. The testing and acceptance of the Winston cones is virtually complete. The testing of the initial batch of HTCC mirrors revealed unexpected variations in the coating performance, including unacceptably low reflectance for several mirrors. The test results have been used by ECI to improve mirror handling, cleaning and coating procedures, and to ultimately improve the final results. The apparatus remains in operation at JLab and will be used to test all 60 of the final production HTCC mirror facets for quality assurance and to provide reflectivity data for future reference.

References

- [1] The CLAS12 Collaboration. CLAS12 Technical Design Report. <http://www.jlab.org/Hall-B/secure/CDR/master.pdf>, 2008.
- [2] J. Beringer et al. Review of particle physics. *Phys. Rev. D*, 86:010001, Jul 2012.
- [3] A. Puckett and M. McClellan. HTCC mirror testing wiki. https://clasweb.jlab.org/wiki/index.php/HTCC_Mirror_and_Winston_Cone_Testing,_Spring_2013, 2013.